

# The AMBRE Project: searching for the closest solar siblings

V. Adibekyan<sup>1</sup>, P. de Laverny<sup>2</sup>, A. Recio-Blanco<sup>2</sup>, S. G. Sousa<sup>1</sup>, E. Delgado-Mena<sup>1</sup>,  
G. Kordopatis<sup>2</sup>, A. C. S. Ferreira<sup>1</sup>, N. C. Santos<sup>1,3</sup>, A. A. Hakobyan<sup>4</sup>, and M. Tsantaki<sup>1</sup>

<sup>1</sup> Instituto de Astrofísica e Ciências do Espaço, Universidade do Porto, CAUP, Rua das Estrelas, 4150-762 Porto, Portugal

e-mail: vadibekyan@astro.up.pt

<sup>2</sup> Université Côte d’Azur, Observatoire de la Côte d’Azur, CNRS, Laboratoire Lagrange, Bd de l’Observatoire, CS 34229, 06304 Nice cedex 4, France

<sup>3</sup> Departamento de Física e Astronomia, Faculdade de Ciências, Universidade do Porto, Rua do Campo Alegre, 4169-007 Porto, Portugal

<sup>4</sup> Byurakan Astrophysical Observatory, 0213 Byurakan, Aragatsotn province, Armenia

Received date / Accepted date

## ABSTRACT

**Context.** Finding solar siblings - stars which formed in the same cluster as the Sun - will yield information about the conditions at the Sun’s birthplace. Finding the lost solar siblings is not an easy task since they are already spread widely around the Galaxy.

**Aims.** In this work we search for solar sibling candidates among the very large spectra-base of solar vicinity stars - AMBRE.

**Methods.** Since the solar siblings have very similar age and chemical abundances as the Sun, we carried out a chemistry and age based search for solar sibling candidates. We used the high-resolution spectra to derive precise stellar parameters and chemical abundances of the stars. We used these spectroscopic parameters together with the Gaia DR2 astrometric data to derive stellar isochronal ages. The Gaia data was also used to study the kinematics of the sibling candidates.

**Results.** From the about 17 000 stars characterized within the AMBRE project we first select 55 stars that have metallicities closest to the solar value ( $-0.1 \leq [\text{Fe}/\text{H}] \leq 0.1$  dex). For these stars we derived precise chemical abundances of several iron-peak,  $\alpha$ - and neutron-capture elements with which to select 12 solar sibling candidates with average abundances and metallicity between  $-0.03$  to  $0.03$  dex. Our further selection left us with four candidates which have stellar ages compatible with the solar age within observational uncertainties. For the two of the hottest candidates we derived the carbon isotopic ratios finding these to be compatible with the solar value. HD186302 is the most precisely characterized and probably the best candidate among our four best candidates.

**Conclusions.** Very precise chemical characterization and age estimation is necessary to identify solar siblings. We propose that besides typical chemical tagging the study of isotopic ratios can give further important information about the relation of sibling candidates with the Sun. Ideally, asteroseismic age determinations of the candidates could solve the problem of imprecise isochronal ages.

**Key words.** stars: abundances, stars: kinematics and dynamics, solar neighborhood

## 1. Introduction

As with most low mass stars, the Sun was probably formed in a cluster (e.g. Lada & Lada 2003) about 4.57 Gyr ago (Bonanno & Fröhlich 2015). The presence of short-lived radioactive isotopes (half-lives shorter than a few Myr), that are mainly products of stellar nucleosynthesis, in the early solar nebula indicates that pollution by a supernova with progenitor mass of  $\sim 20 M_{\odot}$  (Looney et al. 2006), or even higher (e.g.  $\sim 75$ - $100 M_{\odot}$  Williams & Gaidos 2007) occurred in the first epochs ( $\lesssim 2$  Myr) of the Solar life. The existence of such a massive star in the birth cluster of the Sun would require its initial mass to be at least  $500 M_{\odot}$  Weidner & Kroupa (2004) or even  $10^4$  if the progenitor mass of the exploded supernova was  $>75 M_{\odot}$  (Weidner & Kroupa 2004).

Moreover, the dynamical excitement of the trans-Neptunian object Sedna and the Kuiper belt objects (Brown et al. 2004; Morbidelli & Levison 2004) requires

a close encounter with another star in the birth cluster, which also suggested that the solar birth cluster contained  $10^3$ - $10^4$  stars (Adams 2010). Portegies Zwart (2009) suggests that the birth cluster could have a mass between 500 and  $3000 M_{\odot}$  if the size of the cluster was 1-3 pc.

The lifetime of open clusters is typically about 200 Myr (e.g. Piskunov et al. 2006) although it depends on the mass of the cluster (massive clusters live longer) and on the properties of the galaxy (e.g. Lamers & Gieles 2006). The birth cluster of the Sun has therefore long since been dissipated and its members, the solar siblings, are scattered all over the Milky Way (e.g. Bland-Hawthorn et al. 2010).

Finding solar siblings is important for several reasons. It would help us to understand better the origin of our Sun, constrain its birthplace, and the environmental conditions of the Sun’s birth cluster. Moreover, finding and

characterizing planetary systems<sup>1</sup> (e.g. frequency, architecture) around solar siblings could give relevant information about the outcome of planet formation in a common environment. Several attempts have been made to find solar siblings (e.g. Brown et al. 2010; Bobylev et al. 2011; Liu et al. 2015) however, only four plausible candidates have been identified to date: HIP21158, HIP87382, HIP47399, and HIP92831 (Batista & Fernandes 2012; Batista et al. 2014; Ramírez et al. 2014). In most of the solar sibling search studies, the authors started their search from kinematic selection of candidates and then verified if they have metallicities and chemical abundances compatible with the solar ones.

On the contrary, Batista et al. (2014) conducted a search for solar siblings among the HARPS high-resolution FGK dwarfs sample (Adibekyan et al. 2012) using a new approach based on the observed chemical abundance trends with the condensation temperature. The initial HARPS sample used by these authors consisted of about 1,111 stars, the abundances of only 12 elements was used to search for solar chemical twins and finally astrometric data was taken from Hipparcos (van Leeuwen 2007). Batista et al. (2014) found just one candidate solar sibling. Today, we have the possibility to make a new search with improvements in all the mentioned aspects: larger sample, chemical abundances of much more elements, and astrometric data with better precision. All these possibilities are provided by the AMBRE project (de Laverny et al. 2013) and Gaia DR2 (Gaia Collaboration et al. 2018). AMBRE is a Galactic archeology project set up by ESO and the Observatoire de la Côte d’Azur in order to determine the stellar atmospheric parameters for the archived spectra from the ESO spectrographs: FEROS, HARPS, UVES and GIRAFFE. A total of about 230,000 spectra have been homogeneously analyzed.

This paper is organized as follows. In Sect. 2 we describe the initial selection of the sample stars and in Sect. 3 we characterize these stars in terms of stellar parameters (Sect. 3.1), chemical abundances (Sect. 3.3), ages and activities (Sect. 3.4), and kinematics (Sect. 3.5). In Sect. 4 we applied different criteria to select the best solar sibling candidates which we studied in more detail in Sect. 5. We summarize our work in Sect. 6.

## 2. Initial sample selection

Our initial sample is based on the AMBRE project data (de Laverny et al. 2013). Currently, the AMBRE project provides stellar parameters and chemical index  $[\alpha/\text{Fe}]$  for 6,508 FEROS archived spectra (Worley et al. 2012), 10,212 UVES spectra (Worley et al. 2016), and 93,116 HARPS spectra (De Pascale et al. 2014). These spectra correspond to about 17,000 individual stars. The spectra were processed using the MATISSE algorithm (Recio-Blanco et al. 2006), and makes use of a specific grid of synthetic spectra by de Laverny et al. (2012).

<sup>1</sup> Solar siblings can also be good candidates to search for planets with life, if the life transportation between solar systems in the Sun’s birth cluster was efficient (e.g. Adams & Spiegel 2005; Tepfer & Leach 2006). This highly speculative hypothesis that life (biotic materials) can travel in space and “contaminate” new habitats is called panspermia, and in particular the transfer of life between exoplanet systems is called “interstellar lithopanspermia” (von Bloh et al. 2003).

From this initial AMBRE sample we selected 28,631 spectra for which MATISSE parametrization suggests a mean metallicity ( $[M/H]$ ) and  $\alpha$ -element abundance ( $[\alpha/H]$ ) close to the solar value within ( $\pm 0.1$  dex). These spectra correspond to 1,019 unique stars, 987 of which Gaia DR2 (Gaia Collaboration et al. 2018) astrometry is available.

The numerical simulations of Martínez-Barbosa et al. (2016) for solar sibling candidates with parallax  $\varpi > 5$  mas suggest a proper motion ( $\mu$ ) in the range  $4 < \mu < 6$  mas yr<sup>-1</sup> and heliocentric radial velocity (RV) in the range  $-2 < RV < 0$  km/s. We note that these kinematic criteria are only suggestive to increase the probability of finding a solar sibling. Moreover, they are dependent on the assumption of the model of the Milky Way. We decided to apply a very broad initial kinematic criteria in order not to exclude any potential candidate at this stage. From the 987 stars we selected 119 relatively nearby stars ( $\varpi > 5$  mas<sup>2</sup>) which have RV between  $-100$  and  $100$  km/s, and total  $\mu < 50$  mas/yr. We did not consider the distant stars with  $\varpi < 5$  mas (about 10% of the sample stars) because the predictions of kinematic properties of solar siblings are provided for nearby stars. Moreover, most of these distant stars are either very faint (the average V magnitude is  $\sim 11.8$  mag) or evolved massive giant stars ( $M > 1.3 M_{\odot}$ ). The spectra of faint stars are also usually of low quality and it is difficult to derive precise chemical abundances. The massive evolved stars have lifetime smaller than the present-day age of the Sun.

We finally made an intensive literature search for the 119 selected stars and excluded 26 stars belonging to open clusters much younger than the Sun (younger than 100 Gyr). Three stars with effective temperature ( $T_{\text{eff}}$ ) lower than 4500 K were also excluded since our spectroscopic analysis method does not guarantee a derivation of very precise stellar parameters and chemical abundances (at the level of  $\lesssim 0.1$  dex) for these very cool stars. After these selections we ended up with 90 stars that we studied in detail in the next sections.

## 3. Properties of the sample stars

### 3.1. Stellar atmospheric parameters

In this section we describe how we derived precise stellar parameters for the selected 90 stars for which the initial parametrization by MATISSE suggests to be solar sibling candidates. For most of the selected stars, several high-resolution ( $R \sim 100,000$ ) spectra were publicly available at the ESO archive. In order to work with the highest possible quality spectroscopic data we co-added all the available spectra of the stars that were observed with the same instrument and the same setup. For a few stars spectra obtained with different instruments were available and we selected the highest signal-to-noise (S/N)<sup>3</sup> spectra to work with. For one of the stars (HD5418) UVES spectrum that covers only blue wavelengths was available. This wavelength coverage was insufficient to derive the parameters with our technique and this star was thus excluded from the sample.

<sup>2</sup> Following Lindegren et al. (2018) we corrected the parallaxes for the global offset (0.029 mas) and for the  $\sim 30\%$  underestimation of the parallax uncertainties of bright stars (Luri et al. 2018; Arenou et al. 2018).

<sup>3</sup> In this work signal-to-noise refers to S/N per angstrom at around 6000 Å.

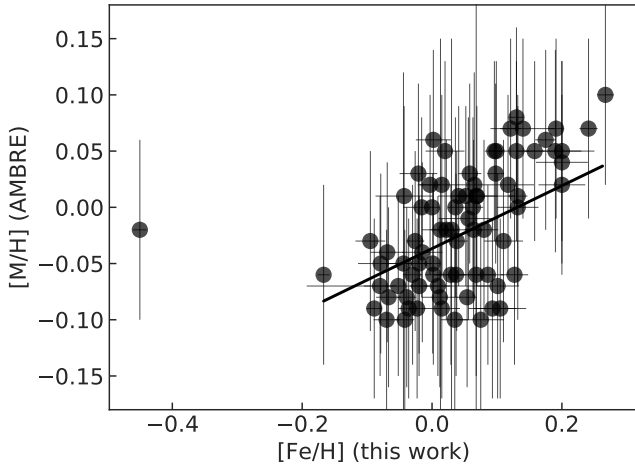


**Fig. 1.** Comparison between AMBRE stellar mean metallicity and  $[\text{Fe}/\text{H}]$  derived in this work from higher S/N spectra. The black solid line shows the result of the weighted least square regression. The star with the lowest  $[\text{Fe}/\text{H}]$  is not included in the fit.

**Table 1.** The main properties of binary system CPD-60315A & CPD-60315B.

Star	CPD-60315A	CPD-60315B
Gaia DR2	4677970179987090304	4677970179988001280
Gmag (mag)	$9.8541 \pm 0.0005$	$9.6830 \pm 0.0006$
$\varpi$ (mas)	$9.5809 \pm 0.0277$	$9.5838 \pm 0.0271$
RV (km/s)	11.9291	11.5168

The co-added spectra were used to derive precise stellar atmospheric parameters ( $T_{\text{eff}}$ ,  $[\text{Fe}/\text{H}]$ ,  $\log g$ , and  $V_{\text{tur}}$ ) for the target stars as in our previous works (Sousa et al. 2008, 2015b). For a detailed description we refer the reader to Sousa (2014). The method is based on classical curve-of-growth analysis where the equivalent widths (EW) of the spectral lines are automatically measured with the ARES v2 code<sup>4</sup> (Sousa et al. 2015a). Under the assumption of local thermodynamic equilibrium (LTE), the parameters were derived by imposing excitation equilibrium and ionization balance for Fe I and Fe II lines. We used the grid of ATLAS9 plane-parallel model of atmospheres (Kurucz 1993) and the 2014 version of MOOG<sup>5</sup> radiative transfer code (Sneden 1973). For stars with  $T_{\text{eff}} < 5200$  K, we derived the parameters using the line-list compiled in Tsantaki et al. (2013). This list represents a selection of lines presented in Sousa et al. (2008) that do not suffer from blends at low temperatures.

For eight stars (HD217738, HD207889, HD217739, HD13021, TYC 964-160-1, BD-114934B, BD-114934B, BD-202665A) the combined spectra had a S/N < 50. The spectroscopic analysis of these low-S/N spectra did not allow to derive very precise stellar parameters and chemical abundances. Our analysis of these stars suggested that they are all more metallic than the Sun by at least 0.1 dex i.e.  $[\text{Fe}/\text{H}] > 0.1$  dex. These stars were excluded from the sample. Moreover, the spectroscopic analysis showed that HD22556

is a spectral binary and it was excluded from the sample. HD66488 and HD110108 were also excluded since we could not derive precise parameters (the method did not converge) for these hot ( $T_{\text{eff}} > 6500$  K) stars. Finally, we decided to exclude HD29167 which is a member of a binary system that consists of two practically identical stars: CPD-60315A and CPD-60315B (see Table 1). The Gaia DR2 astrometry suggests that they have very similar parallaxes (the difference is 0.0029 mas, while the error of parallax for each component is at least 10 times larger), and  $G$  magnitudes (the difference is 0.17 mag). ESO archive contains two HARPS spectra for each of the components with an average S/N  $\approx 30$ . The spectra are almost identical and suggest almost the same RV. It is not very clear whether the individual spectra obtained for each component are not contaminated by the companion. We decided to exclude this star/system from our sample. However, it is a very interesting system to be studied in more detail using higher quality spectra and making sure that the two components are observed separately.

In Fig. 1 we show the comparison between the mean stellar metallicity ( $[\text{M}/\text{H}]$ ) derived by the AMBRE team and the metallicity derived in the current work based on iron lines only ( $[\text{Fe}/\text{H}]$ ). The plot shows that besides an offset of 0.06 dex and a scatter of 0.09 dex, there is a trend: the overestimation of  $[\text{Fe}/\text{H}]$  relative to  $[\text{M}/\text{H}]$  is higher for more metallic stars. This probably reflects the influence of chemical elements other than iron in the definition of the  $[\text{M}/\text{H}]$  index. HD171028<sup>6</sup> is clearly an outlier in this plot. Our literature search confirms that it is a metal-poor star, while AMBRE parametrization resulted to a near solar metallicity. The star has 79 spectra in the ESO archive, 47 of which are parametrized by AMBRE. The AMBRE mean metallicity for this star (excluding the results obtained for the 'outlier' spectrum) is  $\sim -0.64$ , which is even lower than what we report in this work. The same happened for some other stars that show the most discrepant results between AMBRE and this work. It is important to remember that the AMBRE metallicities are derived for individual spectra (sometimes of low quality), while the  $[\text{Fe}/\text{H}]$  in this work is derived from the combined spectra. Without considering HD171028, the mean difference between  $[\text{M}/\text{H}]$  and  $[\text{Fe}/\text{H}]$  is  $0.06 \pm 0.07$  dex<sup>7</sup>. We note that the average error for  $[\text{M}/\text{H}]$  is 0.09 dex and for  $[\text{Fe}/\text{H}]$  is 0.03 dex. Thus the obtained difference is within the errors of our derivations of the metallicity.

A similar difference ( $0.072 \pm 0.10$  dex) between AMBRE  $[\text{M}/\text{H}]$  and  $[\text{Fe}/\text{H}]$  (derived by spectral synthesis method) was observed in Mikolaitis et al. (2017) for a much wider range of stellar metallicities. These authors also stressed that these two parameters are not exactly the same and can be different for stars that have different element-over-iron abundances when compared to the solar values. In order to understand the possible reasons of the observed discrepancies we show in Fig. B.1 the  $[\text{Fe}/\text{M}]$  ratio against the stellar atmospheric parameters, and parameters that could influence the results (e.g. S/N, CCF FWHM as a

<sup>4</sup> The last version of ARES code (ARES v2) can be downloaded from <http://www.astro.up.pt/~sousasag/ares>

<sup>5</sup> The source code of MOOG can be downloaded from <http://www.as.utexas.edu/~chris/moog.html>

<sup>6</sup> This star also belongs to the HARPS metal-poor sample of Santos et al. (2011) and known to host a giant planet (Santos et al. 2007).

<sup>7</sup> In this paper the errors of the mean difference represent the scatter i.e. standard deviation of the differences. To derive the standard error of the mean one should divide these values by square root of the sample size.

proxy of rotational velocity). This ratio, besides metallicity, correlates with the microturbulent velocity, effective temperature and CCF FWHM (Full-Width-Half-Maximum of Cross Correlation Function). In addition, we also derived the stellar parameters with our EW method using the individual spectra of the stars that were used in the AMBRE project. The comparison between the metallicities derived from individual and co-added spectra is shown in Fig. B.2. The plot shows a very good agreement, which suggests that the slightly discrepant results obtained between AMBRE project and this work is probably related to the methods of the derivation of stellar parameters.

Similar to stellar metallicity, in Figs. B.3 and B.4 we compared the surface gravity and  $T_{\text{eff}}$  derived by AMBRE team and in this work. For  $\log g$  we observed a negligible offset of 0.03 dex and a scatter of 0.22 dex. This scatter can be explained with the average errors of 0.25 dex and 0.06 dex reported for AMBRE and in this work, respectively. For the  $T_{\text{eff}}$  we observed a good agreement between the two works. The  $41 \pm 91$  K difference is within the reported errors of 96 and 33 K for AMBRE and this work, respectively.

For the further search of the best solar sibling candidates, we restricted our final sample to the stars with  $-0.1 \leq [\text{Fe}/\text{H}] \leq 0.1$  dex, which leaves us with a sample of 55 stars. The stellar parameters of these stars are presented in Table A.1. We note that only 23 of these stars were included in the search of solar sibling by Batista et al. (2014).

### 3.2. Trigonometric surface gravity

A known difficulty of spectroscopic methods is that they cannot constrain stellar surface gravity with a good accuracy (typically lower than  $\sim 0.2$  dex e.g. Sozzetti et al. 2007; Kordopatis et al. 2011; Mortier et al. 2013; Tsantaki et al. 2014). It has been shown that the spectroscopic surface gravity derived with the assumption of LTE ionization balance is not always in good agreement with the  $\log g$  derived from the transit light curves of exoplanet host stars and asteroseismology (e.g. Mortier et al. 2014). A clear disagreement is also observed between spectroscopic and trigonometric surface gravities (e.g. Tsantaki et al. 2013; Bensby et al. 2014; Delgado Mena et al. 2017). This observed difference between spectroscopic and trigonometric  $\log g$  depends on the  $T_{\text{eff}}$  of the stars (e.g. Delgado Mena et al. 2017). We believe that the trigonometric  $\log g$  values better represent the real surface gravity of the stars since they follow much better the isochrones in the Hertzsprung-Russell (HR) diagram when compared to the spectroscopically derived ones (see e.g. Delgado Mena et al. 2017). Thus we decided to derive trigonometric  $\log g$  for the sample stars using the Gaia DR2 astrometric data. We note that if no trigonometric  $\log g$  is available one can alternatively use the corrections of spectroscopic surface gravities proposed by Mortier et al. (2014). Since all the targets are bright stars from the solar vicinity, Gaia provides very accurate parallaxes. Only four stars out of the 55 have relative error in  $\varpi$  worse than 2%, with the largest error being 6.4%.

We calculated the trigonometric  $\log g$  using the well known Newton's law of universal gravitation and Stefan-Boltzmann law (see e.g. Eq. 1 from Santos et al. 2004). We used the Gaia DR2 parallaxes (Gaia Collaboration et al.

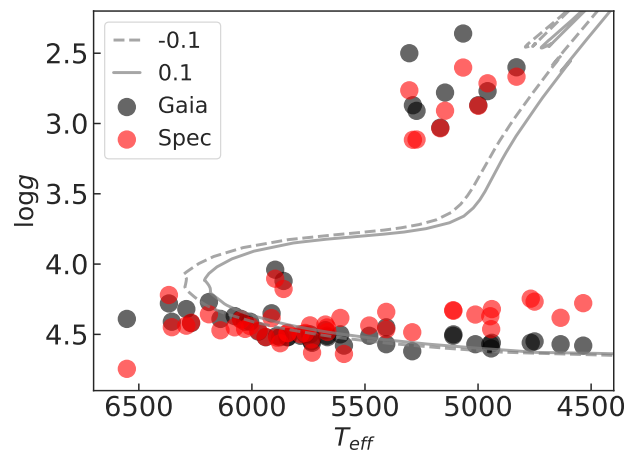


**Fig. 2.** HR diagram for the sample stars with the spectroscopic (Spec) and trigonometric (Gaia) surface gravities. The solar age isochrones for stars with metallicity  $-0.1$  and  $0.1$  dex are shown in gray.

2018), V magnitudes extracted from Simbad<sup>8</sup>, bolometric corrections based on Flower (1996), and revisited by Torres (2010), the stellar masses and spectroscopic  $T_{\text{eff}}$ . Stellar masses, together with the radii and ages of the stars, are derived from the PARAM v1.3 web interface<sup>9</sup> based on the Padova theoretical isochrones from Bressan et al. (2012) and with the use of a Bayesian estimation method (da Silva et al. 2006). As input parameters for PARAM we used the V mag,  $\varpi$ , and spectroscopic  $T_{\text{eff}}$  and  $[\text{Fe}/\text{H}]$ . As priors for the mass, the initial mass function of Chabrier (2001) was used. No correction for interstellar reddening is needed since all the stars are nearby objects within 200 pc. The results are presented in Table A.1.

In Fig.2 we show the spectroscopic HR diagram for the sample stars together with the Padova isochrones for solar age and metallicity. The plot clearly demonstrates that the spectroscopic  $\log g$  values do not follow the expected stellar evolution curves for cool dwarfs. It is also clear that the evolved stars are too far from the solar age isochrones (they are mostly very young: see Sect. 3.4).

### 3.3. Chemical abundances

When deriving chemical abundances of the elements we generated the model atmospheres for the spectroscopically derived  $T_{\text{eff}}$  and  $[\text{Fe}/\text{H}]$ , and the trigonometric  $\log g$ . We did not re-derive the  $T_{\text{eff}}$  and  $[\text{Fe}/\text{H}]$  by fixing the  $\log g$  since the effect of an unconstrained  $\log g$  on the derivation of other stellar parameters is small for the EW-based curve-of-growth approach (Torres et al. 2012; Mortier et al. 2013). Moreover, although the effect is not very strong, fixing the  $\log g$  can bias the results and derivation of other atmospheric parameters (Mortier et al. 2014; Smalley 2014).

The derivation of chemical abundances was done as in our previous works (e.g. Adibekyan et al. 2012; Delgado Mena et al. 2017). We used the same tools and models of atmospheres as for the derivation of stellar parameters. For elements with only a few spectral lines the EW measure-

<sup>8</sup> <http://simbad.u-strasbg.fr/simbad/>

<sup>9</sup> <http://stev.oapd.inaf.it/cgi-bin/param>

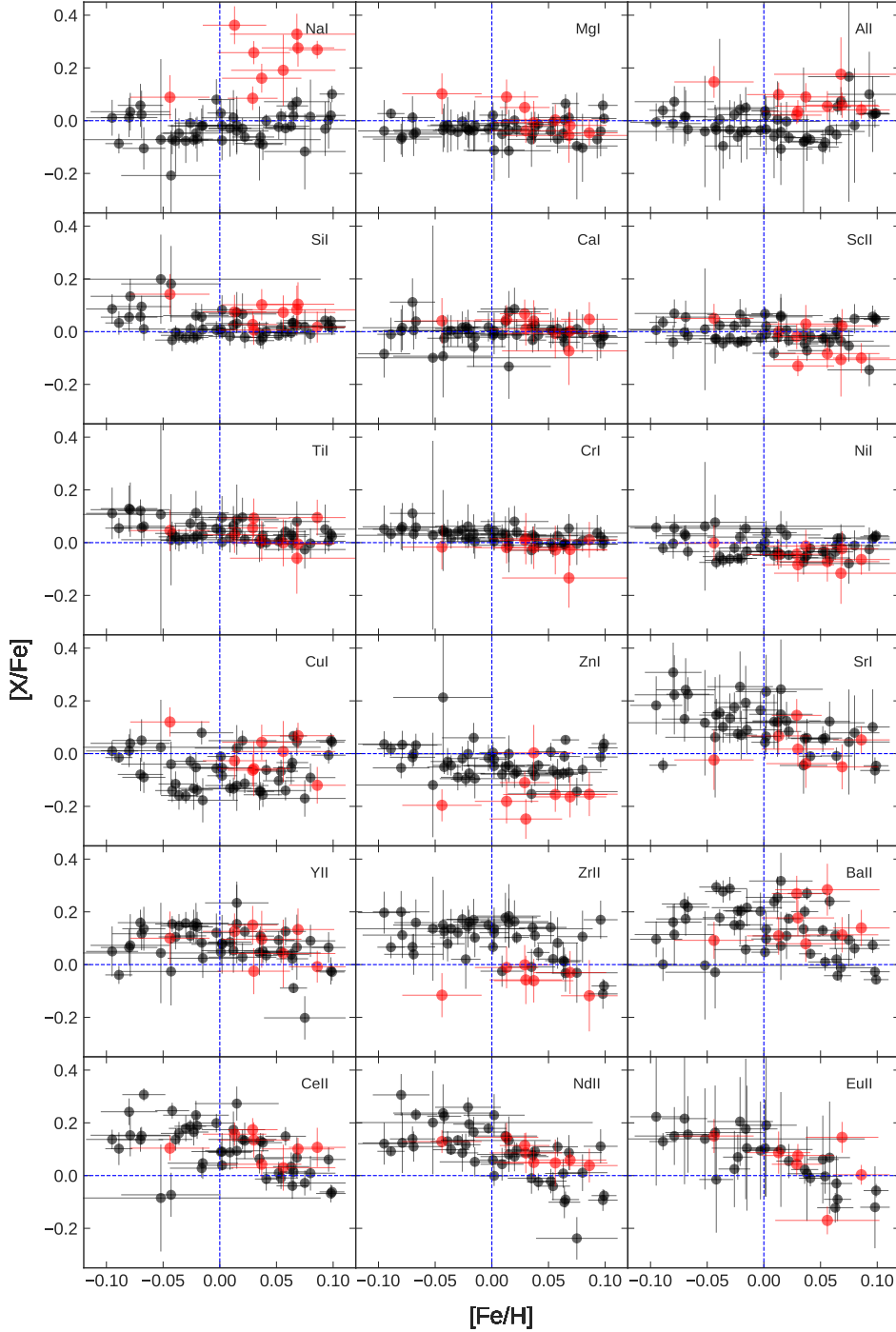


**Fig. 3.** Abundance ratio for a range of species X,  $[X/Fe]$  against stellar metallicity for the current sample. The evolved (and also massive) stars with surface gravity  $< 3.5$  dex are shown in red, and the stars at earlier stages of their evolution ( $\log g > 3.5$  dex) are shown in black. The blue dashed horizontal and vertical lines show the solar abundances.

ments of ARES was done with careful visual inspection of the spectra. In a very few cases, when the ARES measurements were obviously wrong (e.g., as a result of a presence of cosmic rays or bad pixels close to the spectral line), we manually measured the EWs using the task `splot` in IRAF<sup>10</sup>. The final abundances of the elements with more than three

measured spectral lines were calculated as a weighted mean of the estimates from each line, where the inverse of the distance from the median abundance was considered as a weight. This method can be effectively used without removing suspected outlier lines (Adibekyan et al. 2015a). For the elements with two or three lines only we calculated the errors on EWs following Cayrel (1988) to provide more realistic errors for the abundances of elements. This uncertainty takes into account the statistical photometric error due to the noise in each pixel and the error related

<sup>10</sup> IRAF is distributed by National Optical Astronomy Observatories, operated by the Association of Universities for Research in Astronomy, Inc., under contract with the National Science Foundation, USA.



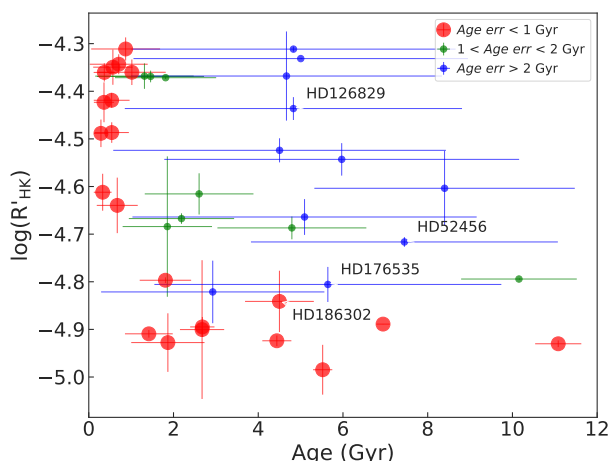


**Fig. 4.** The stellar activity index  $\log(R'_{\text{HK}})$  against ages for the stars with masses less than  $1.2 M_{\odot}$ . The names of the four best candidates are indicated in the plots.

to the continuum placement. The later has the dominant contribution to the total error (Cayrel 1988; Bertran de Lis et al. 2015). These errors are then propagated to derive the abundance uncertainties for each spectral line. The final uncertainties for the average abundance are propagated from the individual errors. The final errors of the  $[X/H]$  abundances are calculated as a quadratic sum of the errors due to EW measurements and errors due to uncertainties in the atmospheric parameters. The solar reference abundances are taken from Adibekyan et al. (2016) and Delgado Mena et al. (2017) which were derived using the combined HARPS reflected spectrum ( $S/N \sim 1300$ ) from Vesta which we extracted from the ESO public archive. We note that the choice of asteroids to obtain the solar reflected spectra and observations at different epochs have effects smaller than  $< 0.01$  dex (e.g. Bedell et al. 2014).

In Figs. 3 and C.1 we show the dependence of  $[X/Fe]$  abundance ratios on the metallicity, trigonometric surface gravity and effective temperature. The massive and evolved stars ( $\log g < 3.5$  dex and  $M > 1.5 M_{\odot}$ ) of the sample are shown in red and the dwarf solar-type stars are in black. The abundance of all the stars will be presented in an electronic readable table at the CDS. We note, that for two relatively fast rotator stars (HD75006 and HD62816) we were not able to derive abundances of all the elements.

### 3.4. Stellar ages and activity

One of the main parameters for identifying solar siblings is the stellar age, as the solar siblings are expected to share the same age. As discussed in Sec. 3.2, the stellar ages for the sample stars were derived using the Padova isochrones (Table A.2). Although the precise astrometric data of Gaia helps to increase the precision of stellar ages, unfortunately, for a significant fraction of the stars the uncertainties of the age estimations are still  $> 2-3$  Gyrs.

There are several stellar parameters that correlate with stellar age. These chronometers can be used, at least, to cross-check the isochronal ages of the stars. Among the most discussed chronometers is the  $\log(R'_{\text{HK}})$  chromospheric activity indicator (e.g. Mamajek & Hillenbrand 2008; Pace 2013; Lorenzo-Oliveira et al. 2016, 2018). We followed the works of Suárez Mascareño et al. (2015) and

Hojjatpanah et al. (2018, in prep) to measure the emission flux in the cores of the Ca II H&K lines and determine the activity index. For most of the stars we had HARPS spectra available which covers the wavelength region of Ca II lines. However, for two stars (HD209458 and HD92987) high resolution UVES spectra that were used to spectroscopically characterize the stars did not cover the Ca II lines. To determine the activity indexes of these stars we used the HARPS-N<sup>11</sup> spectrum for HD209458 and the  $R = 58,000$  resolution UVES spectrum that covered 3732-4999Å region for HD92987. The activity indices of the stars can be found in Table A.2.

In Fig. 4 we show the dependence of stellar activity with age for the stars with masses  $< 1.2 M_{\odot}$ . This mass limit corresponds to  $\sim F3$  spectral type. Stars of spectral types earlier than  $\sim F4$  have shallower convection zones and do not show correlation between stellar activity, rotation, and age (e.g. Wolff et al. 1985; Garcia-Lopez et al. 1993). Moreover, most of these massive stars are already evolved from the main-sequence (MS) for which the age-activity relation is probably not valid (Wright et al. 2004). The figure clearly shows that all the active stars ( $\log(R'_{\text{HK}}) \lesssim -4.7$  dex) with age estimations with errors  $< 1$  Gyr are younger than about 1.5 Gyr. One can also easily identify the group of active stars that have isochronal ages older than 4 Gyr. These later stars are those with the largest errors in the age.

Besides the chromospheric activity, one can also use some abundance ratios, such as  $[Y/Mg]$ , (e.g. Nissen 2015; Tucci Maia et al. 2016; Slumstrup et al. 2017; Delgado Mena et al. 2018, Titarenko et al., 2018 submitted), and Li abundance (e.g. Sestito & Randich 2005; Charbonnel & Talon 2005; Andr  ssy & Spruit 2015) as an indicator of stellar age. We use these chronometers to verify the robustness of the derived ages for the best solar sibling candidates in Sect. 4.

### 3.5. Kinematics

During its evolution the Sun's birth cluster can undergo many disruptive processes (e.g. dissolution of the cluster, non-axisymmetric perturbations due to the presence of the bar and spiral arms) leading to spreading of the solar siblings around the Milky Way. Several studies provided predictions on the current distribution of the solar siblings (e.g. Bland-Hawthorn et al. 2010; Brown et al. 2010; Bobylev & Bajkova 2014; Mart  nez-Barbosa et al. 2016). Depending on the assumptions about the Galactic model and the number of stars in the initial cluster, different number of solar siblings are suggested to be currently present in the solar neighborhood (Bland-Hawthorn et al. 2010; Mart  nez-Barbosa et al. 2016). These solar siblings are also predicted to have a given kinematics (Bobylev et al. 2011), Galactic coordinates (e.g. Bland-Hawthorn et al. 2010), and phase-space distribution (Mart  nez-Barbosa et al. 2016).

We calculated the Galactic space velocity components (UVW) by combining the Gaia astrometric data and the RV derived in the current work. When calculating the velocity components with respect to the local standard of rest (LSR), for the solar motion relative to the LSR we adopted the values of  $(U, V, W)_{\odot} = (11.1, 12.24, 7.25)$  km s<sup>-1</sup> as measured by Sch  nrich et al. (2010). The or-

<sup>11</sup> HARPS-N is the northern copy of HARPS and has the same resolution and same spectral coverage (Cosentino et al. 2012).

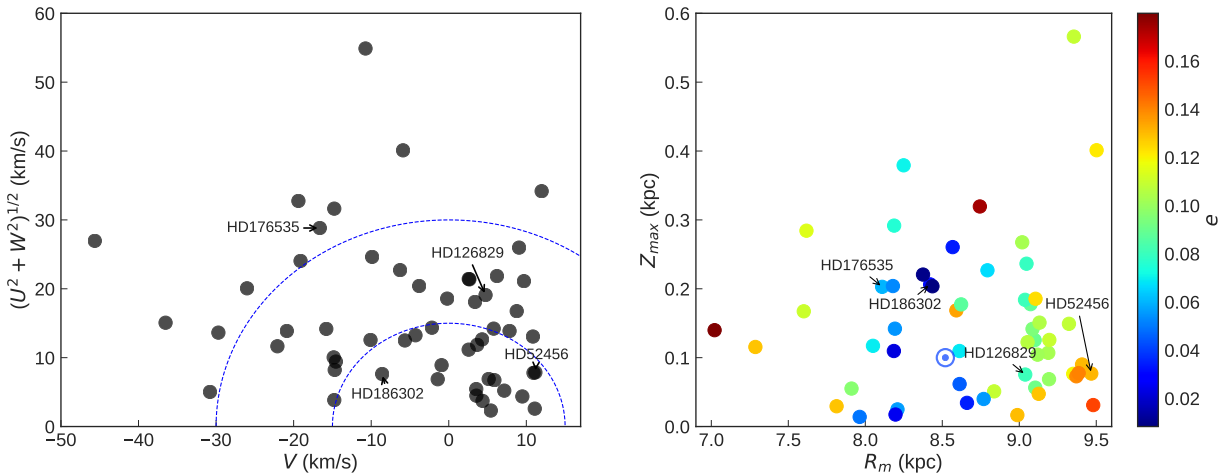


**Fig. 5.** *Left panel:* The distribution of the velocities of our sample Solar sibling candidates in the Toomre diagram. *Right panel:*  $Z_{\text{max}}$  (maximum height from the Galactic plane) versus  $R_m$  (mean orbital radius) for the sample stars. The colour-bar corresponds to the orbital eccentricities of the stars. The position of the Sun is marked by the solar symbol. The four best Solar sibling candidates are indicated by their names in the plots.

bit parameters of the sample stars were also derived by using the space velocities and the publicly available package `galpy`<sup>12</sup> (Bovy 2015). We used the axisymmetric potential `MWPotential2014` (Bovy 2015), and assumed  $R_{\odot} = 8.34$  kpc and  $Z_{\odot} = 0.025$  kpc (Reid et al. 2014).

In the left panel of Fig. 5 we show the distribution of the stars in the Toomre diagram. The velocities of the stars are relative to the Sun. We also show the isovelocity curves of  $V_{\text{pec}} = (U^2 + V^2 + W^2)^{1/2} = 15$  km s<sup>-1</sup> and  $30$  km s<sup>-1</sup>. The right panel of the same figure shows the dependence of the maximum height from the Galactic plane ( $Z_{\text{max}}$ ) versus the mean orbital radius ( $R_m$ ), colour-coded by their eccentricities ( $e$ ). The position of the Sun is also shown in the figure. Note, that the kinematic parameters of the Sun are calculated using `galpy` following the instructions in the manual of the package. The kinematic properties of the stars are presented in Table A.3.

#### 4. Selecting the best solar sibling candidates

After the derivation of the main properties for the sample stars we can select the best solar sibling candidates. The two main and very strict conditions for solar siblings are i) to be chemically similar to the Sun and ii) to have the same age as the Sun.

##### 4.1. Siblings by chemistry

The level of chemical similarity between the solar siblings depends on the chemical homogeneity of the Sun's birth cluster. Some theoretical works suggest that open clusters are chemical homogeneous up to  $\sim 10^5 M_{\odot}$  in mass (e.g. Bland-Hawthorn et al. 2010). Very recent work by Armillotta et al. (2018) suggests that the spatial scale of the chemically homogeneous clusters consisting of about 2000 stars is  $\sim 1$  pc. Note, that the typical diameter of open clusters is a few parsec (Schilbach et al. 2006). The observed variation of chemical abundances in open clusters (star-to-star abundance scatter) due to turbulent mixing in star-forming molecular clouds is much smaller than the initial

gas abundance scatter where the stars were formed (e.g. Feng & Krumholz 2014). Most recent observational studies suggest that open clusters are homogeneous at about 0.03 dex level (e.g. Hogg et al. 2016; Liu et al. 2016b; Bovy 2016).

In Fig. C.2 we show the chemical abundances of the stars as a function of atomic number. One can clearly see that some stars show a systematic over- or under-abundance in heavy elements ( $Z > 30$ ) when compared to the light elements. This high or low heavy-to-light element ratio relative to the solar value is probably a consequence of galactic chemical evolution. The interstellar medium becomes polluted in neutron-capture elements by stars at the asymptotic giant branch (AGB) phase. Thus stars with different ages might show different abundance ratios of light-to-light elements (e.g. Meléndez et al. 2014; Spina et al. 2016). In addition the enhancement of neutron-capture elements for an individual star can be due to a pollution from a companion AGB star (Liu et al. 2016a).

To identify the solar sibling candidates we selected the stars which have metallicities, and average chemical abundances of light and heavy elements close to the “solar cluster value” within the uncertainties. Because of the aforementioned (possible) chemical inhomogeneity of the Sun's birth cluster we assumed the “solar cluster value” for chemistry to be within  $0.00 \pm 0.03$  dex. The average chemical abundances of the light and heavy elements were calculated as the weighted mean by using inverse of the uncertainties of individual abundances as weights. For evolved massive stars we did not consider the abundance of Na when calculating the mean abundances because of its overabundance when compared to the dwarfs (see Fig. C.1 and e.g. Adibekyan et al. 2015b). The overabundance of Na in giant stars is usually explained as a stellar evolutionary effect<sup>13</sup> (e.g. Jacobson et al. 2007), although an inappropriate spectroscopic analysis method (e.g. not taking into account non local thermodynamic equilibrium effects which are stronger for

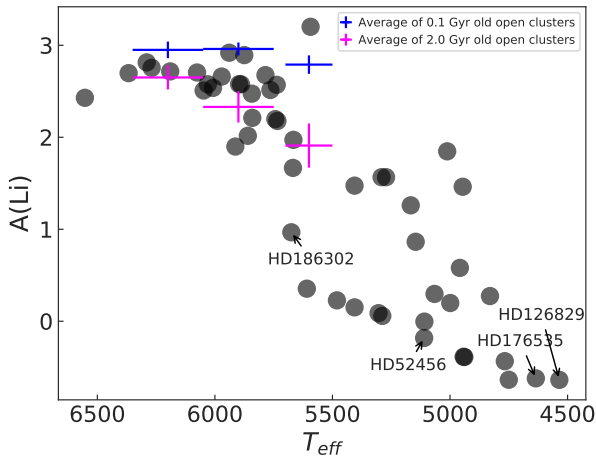
<sup>13</sup> Note that the very recent work by Smiljanic et al. (2016) suggests that the Na abundance of stars with masses below  $\sim 2 M_{\odot}$  is not affected by internal mixing processes.

<sup>12</sup> <http://github.com/jobovy/galpy>

**Table 2.** The stellar ages based on different chemical abundance ratios for our best sibling candidates.

Star	Age([Y/Mg]) <sup>1</sup> Gyr	Age([Y/Si]) <sup>1</sup> Gyr	Age([Y/Mg]) <sup>2</sup> Gyr
HD186302	3.1±1.7	2.4±1.6	3.8±1.7
HD126829	3.5±3.3	9.4±5.1	4.2±3.4
HD176535*	—	7.8±4.5	—
HD52456	1.0±2.5	2.6±2.4	1.5±2.6

\*No [Mg/H] abundances was derived for this star.

<sup>1</sup>Based on Delgado Mena et al. (2018, in prep).<sup>2</sup>Based on Tucci Maia et al. (2016).**Fig. 6.** Li abundance versus stellar effective temperature for the sample stars. The four best candidates are indicated by their HD numbers. The average Li abundances for 0.1 Gyr and 2.0 Gyr open clusters (Pleiades/Blanco1 and Hyades/Praesepe/Coma Ber/NGC 6633) in three ranges of  $T_{\text{eff}}$  are also shown. The data are taken from Sestito & Randich (2005).

giants than for dwarfs (Alexeeva et al. 2014) can also affect the results.

Our chemical and metallicity selection criteria left us with 12 stars: HD2247, HD45415, HD52456, HD62412, HD74006, HD77191, HD99648, HD115341, HD126829, HD176535, HD186302, HD199951.

#### 4.2. Siblings by age

Very recently, Ness et al. (2018) demonstrated that at solar metallicity ( $[\text{Fe}/\text{H}] = 0.00 \pm 0.02$  dex) 1% of field star pairs can have indistinguishable chemical abundances at a 0.03 dex precision level. Thus being chemically identical to the Sun is an important and mandatory criterion, but definitely not enough to identify stellar siblings. In this section we aimed at selecting the candidates that have ages compatible to the age of the Sun.

From the 12 selected candidates five stars (HD45415, HD62412, HD74006, HD99648, HD199951) have  $M > 1.65 M_{\odot}$ . The lifetime of these stars is therefore shorter than the current age of the Sun and thus they cannot be solar siblings. Three other stars have isochronal ages shorter than 3 Gyr:  $0.65 \pm 0.50$ ,  $1.46 \pm 1.26$ , and  $2.67 \pm 0.52$  Gyr for HD2247, HD77191, and HD115341, respectively. These three stars were thus excluded from the sample of best candidates.

The remaining four stars (HD52456, HD126829, HD176535, HD186302: see table 2) have isochronal ages similar to the Sun within the uncertainties. It is important to note, that except for HD186302, the uncertainties of isochronal ages are larger than 3.5 Gyr (see Table A.2 which makes very difficult to conclude whether they are solar siblings or not. One of these stars (HD126829) seems to be very active for a solar age dwarf:  $\log(R'_{\text{HK}}) = -4.4$  dex. This cool K-type star has a B–V colour out of the range for which Mamajek & Hillenbrand (2008) have calibrated their age-activity relation and thus we cannot use this chronometric indicator. The relation between chromospheric activity and rotation (and age) is probably more complex when one moves towards much cooler temperatures than the Sun (e.g. Noyes et al. 1984; Suárez Mascareño et al. 2016). However, we were able to use the age-activity relation of Mamajek & Hillenbrand (2008) to derive the ages of HD186302 and HD52456, which are 3.8 and 2.2 Gyr, respectively. Note that the errors on this age can be 30-60% depending on the activity level of the star (Mamajek & Hillenbrand 2008).

As an independent chronometer we also examined the Li abundance of these four stars. The Li abundances of the sample stars were derived from the EW measurements of the Li I 6708 Å line. We note that for an accurate Li abundance derivation one usually uses the spectral synthesis method (as it has been done in our previous works e.g. Delgado Mena et al. 2014, 2015). However, for the purpose of verification of the stellar ages the fast EW method is sufficient. In Fig. 6 we show the relation between Li abundance and  $T_{\text{eff}}$ . The plot suggest that all four stars, including the active star HD126829, are not particularly young ( $< 2$  Gyr).

Moreover, as we mentioned in Sect. 3.4, [Y/Mg] and [Y/Si] ratios can also be used to estimate the stellar ages. We used the relation between [Y/Mg] and age, and [Y/Mg] and age provided in Delgado Mena et al. (2018, in prep), and the [Y/Mg] vs age relation from Tucci Maia et al. (2016). The results are presented in Table 2. Unfortunately, the errors of the age estimates are large and they cannot be used to further constrain the ages. Nevertheless, the abundances of HD52456 suggest a young age ( $< 3$  Gyr) for this star. We note that the relations in Delgado Mena et al. (2018, in prep) and Tucci Maia et al. (2016) are obtained for solar-analogs and solar-twins, and do not cover the temperatures of the three coolest stars in our sample. Thus, the age estimates for these three stars derived by this method should be taken with more caution.

Unfortunately, the uncertainty of the age estimations based on the activity and chemical abundances are very large and do not help significantly in making a better selection on these last candidates.

### 5. The four best sibling candidates

In the previous sections we identified four solar sibling candidates that have chemical abundances (see Fig. 7) and ages similar to that of our Sun. In this section we will explore the kinematic properties and the carbon isotopic ratio of these targets.



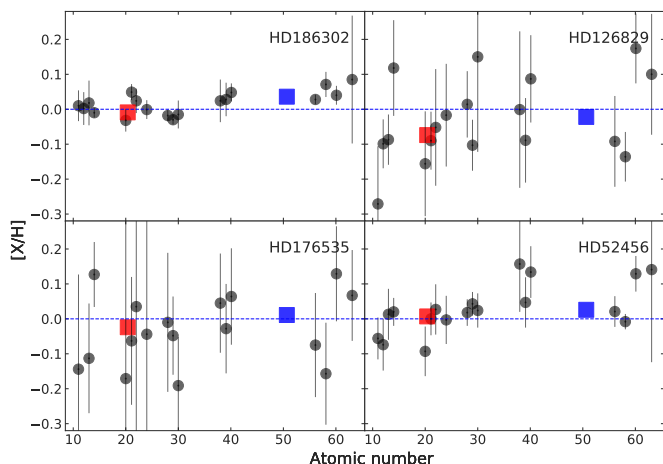


**Fig. 7.** Abundances versus atomic number for the four best solar sibling candidates. The average abundances of light ( $Z \leq 30$ ) and heavy ( $Z > 30$ ) elements are shown by red and blue squares, respectively.

### 5.1. Kinematics and orbits

As mentioned in Sect. 3.5, several attempts have been made to predict the present-day kinematics and orbits of the solar siblings. These predictions are highly dependent on the used model of the Galaxy and the initial properties (e.g. mass and position in the Galaxy) of the parent cluster (see e.g. Bland-Hawthorn et al. 2010; Martínez-Barbosa et al. 2016, for details and discussion).

In terms of the peculiar velocity and orbital parameters HD186302 seems to be the closest one to the Sun (see Fig. 5). HD176535 is the furthest one in terms of peculiar velocity and HD52456 in terms of galactic orbital parameters. It is clear that this kinematic analysis is only very qualitative. For a quantitative kinematic study one should construct the Galactic orbits of these candidates and integrate the orbits backwards in time to see if their orbits encountered with the orbit of the Sun about 4.6 Gyr ago. An obvious limitation of this technique is that serious assumptions should be made about the model of the Milky Way.

### 5.2. Carbon abundances and isotopic ratios

We also tried to estimate LTE carbon abundances and carbon isotopic ratios ( $^{12}\text{C}/^{13}\text{C}$ ) by spectral synthesis for our best sibling candidates. The carbon isotopic ratio is indeed another good indicator of the initial composition of the parent cluster, since this ratio is expected to have not varied at all in the atmosphere of dwarf stars (a strong decrease of  $^{12}\text{C}/^{13}\text{C}$  is only expected after the first dredge-up in low-mass stars). We also remind that isotopic ratios are insensitive to atmospheric parameter uncertainties because one compares lines originating from identical molecular excitation levels. Moreover,  $^{12}\text{C}/^{13}\text{C}$  ratio changes with galactocentric distance (e.g. Wilson & Matteucci 1992) and time (e.g. Kobayashi et al. 2011) and, thus, this ratio could help to characterize the parent cluster. In summary, if close to Solar carbon abundances and  $^{12}\text{C}/^{13}\text{C}$  ratios are found for our best candidates, their solar sibling nature could then be reinforced.

For such abundance derivations, we analyse the co-added HARPS spectra of our best candidates around the G-band where several  $\text{C}^{12}\text{H}$  and  $\text{C}^{13}\text{H}$  features are expected to be present. Very high resolution and high S/N spectra are required for such an analysis since the  $^{13}\text{CH}$  lines are expected to be very weak in metal-rich cool dwarfs because most ( $\sim 99\%$ ) of the carbon is  $^{12}\text{C}$ . Moreover, one also needs to adopt a very good linelist for the spectral synthesis since there are almost no isolated  $^{13}\text{CH}$  lines in such spectra and one has thus to play with several blends. Finally, the spectra of metal-rich cool dwarfs are also difficult to normalize in this spectral domain. Due to such difficulties, no previous determinations of carbon isotopic ratios in metal-rich cool-dwarfs from CH lines have been found in the literature. However, some carbon abundance derivations in such dwarfs are reported (e.g. Suárez-Andrés et al. 2017) since the pioneering works of Pagel (1964) and Cohen (1968). Some measurements of carbon isotopic ratios are reported in giant stars with lower  $^{12}\text{C}/^{13}\text{C}$  ratios, and thus stronger  $^{13}\text{CH}$  lines (see for instance Sneden et al. 1986; Aoki et al. 2006).

Our analysis has been conducted by computing synthetic spectra with the TURBO spectrum code (Alvarez & Plez 1998) and MARCS model atmospheres (Gustafsson et al. 2008) interpolated at the stellar parameters of the sibling candidates. We adopted the CH linelist (including  $^{12}\text{CH}$  and  $^{13}\text{CH}$  lines) from Masseron et al. (2014) and Vienna Atomic Line Database<sup>14</sup> (VALD; Piskunov et al. 1995; Kupka et al. 1999; Ryabchikova et al. 2015). First, we estimated the carbon abundance by comparing the synthetic and observed spectra over a large wavelength domain around the G-band (typically from 4290 to 4320 Å). Then, the carbon abundance being fixed, we carefully examined a couple of spectral regions where the  $^{13}\text{CH}$  lines are predicted to be stronger. We point out that, since the  $\text{C}^{13}\text{H}$  lines become extremely weak for  $^{12}\text{C}/^{13}\text{C}$  ratios larger than  $\sim 60$ , only a lower limit can be estimated. To validate our procedure, we first analysed a HARPS spectrum of Vesta and derived  $A(\text{C}) = 8.35$  and lower limit of  $^{12}\text{C}/^{13}\text{C} \gtrsim 70$  for the Sun in agreement with the reference Solar values:  $A(\text{C}) = 8.39$  dex (Asplund et al. 2005) and  $^{12}\text{C}/^{13}\text{C} = 86.8$  (Scott et al. 2006). This methodology allowed us to derive a carbon abundance equal to 8.40 and 8.35 dex for HD186302 and HD52456, respectively (i.e. a carbon abundance very close to the Solar one, confirming their probable sibling nature). Furthermore, their carbon isotopic ratio is found to be larger than  $\sim 50$ -60. As for the Solar spectrum, their  $^{13}\text{CH}$  lines are too weak to well analysed them in crowded spectra that are difficult to normalize. Moreover, because of such difficulties, it was impossible to derive abundances for the spectra of our two other sibling candidates since they are even cooler and thus suffer from much stronger blends and normalisation problems. In any case, the reported carbon abundances and upper limits for the  $^{12}\text{C}/^{13}\text{C}$  ratio in HD186302 and HD52456 are in agreement with being solar siblings.

## 6. Summary

As discussed in the introduction, finding solar siblings will help us to better understand the environment where our Sun has been formed. The search of solar siblings is difficult

<sup>14</sup> VALD: <http://vald.inasan.ru/vald3/php/vald.php>

since these stars are expected to be already spread over the Milky Way. Only handful solar siblings are expected (depending on how they are dispersed around the Galaxy) to be found in the solar vicinity (Portegies Zwart 2009). Moreover, most of these siblings should have low masses (due to initial-mass function) and thus be faint (Martínez-Barbosa et al. 2016) to find and then to precisely characterize. Since by definition solar siblings are the stars which were formed with the Sun in the same cluster, they must have i) chemical abundances very similar to the solar ones (if the stellar evolution did not affect the atmospheric chemical composition) and ii) the same age as the Sun. In addition, they should have present-day kinematics suggesting that they have been formed in the same location as the Sun. The predictions about the kinematics and orbits of solar sibling in the vicinity of our Sun is not trivial and heavily depends on the characteristics of the solar birth cluster (e.g. size, location etc) and the adopted Galactic model. In this work we carried out mostly a chemical and age based search of solar siblings among the AMBRE stars located within about 200 pc ( $\varpi \geq 5\text{mas}$ ). The selected sibling candidates were then briefly studied to understand how close are they to the Sun in terms of kinematics.

Out of about 17,000 stars characterized within the AMBRE program, we selected 55 stars that have stellar metallicity ( $[\text{Fe}/\text{H}]$ ) from  $-0.1$  to  $0.1$  dex. For these stars we derived the chemical abundances of several iron-peak,  $\alpha$ -capture, and neutron-capture elements. Then we selected 12 stars that have average abundances and metallicity very similar to that of the Sun (by  $\pm 0.03$  dex).

Derivation of the stellar ages of these 12 sibling candidates by chemistry allowed us to narrow down to a sample of four candidates that have ages similar to the Sun within the uncertainties. The ages of the stars have been derived by isochrone fitting. Additional independent age indicators (such as chromospheric activity, Li abundance, and age-sensitive abundance ratios) have been also used to confirm or infirm the isochronal ages of the stars with large uncertainties. Among the four selected stars HD186302 is the only one which has an isochronal age error of less than 1 Gyr. The other three candidates have error in age of greater than 3 Gyr.

Our very simple kinematic study of the four best candidates suggested that HD176535 might be the least likely candidate and HD186302 the most likely candidate in terms of kinematics.

As a final test we derived the carbon isotopic ratio for the two of the hottest ( $T_{\text{eff}} > 5000$  K) candidates which were compatible with the solar value. We suggest that other isotopic ratios sensitive to Galactic chemical evolution such as  $^{24}\text{Mg}/^{25}\text{Mg}$  and  $^{25}\text{Mg}/^{26}\text{Mg}$  (Kobayashi et al. 2011) can be used to identify solar siblings. For example, Yong et al. (2004) have already studied the  $^{24}\text{Mg}/^{25}\text{Mg}$  and  $^{25}\text{Mg}/^{26}\text{Mg}$  ratios in Hyades cool dwarfs and found a good agreement in the values of isotope ratios among the stars belonging to the cluster.

We note that we did not consider some important astrophysical effects such as atomic diffusion and extra mixing mechanisms that can affect the atmospheric abundances of the stars during their evolution and also influence on the derivation of their isochronal ages (e.g. Dotter et al. 2017). We also did not consider the possibility of the change in stellar surface abundances due to planet engulfment and/or planet formation (Smith et al. 2001; Meléndez et al. 2009;

Ramírez et al. 2010). Some theoretical works support the possible modification of stellar abundances due to planet formation (e.g. Kunitomo et al. 2018; Chambers 2010), (but see also Théado & Vauclair 2012; Gustafsson 2018). However, from observational point of view the presence of chemical signatures of planet formation in the spectra of stars is still under a lively debate (see e.g. Adibekyan et al. 2014, 2017, and references therein).

In summary we identified four solar sibling candidates among the AMBRE data. Because of its relatively high temperature ( $T_{\text{eff}} = 5675$  K), HD186302 is the most precisely characterized star among the four. Interestingly, HD176535 has been already identified as a solar sibling candidate by Batista et al. (2014). The other three candidates are cooler which lead to larger errors in the atmospheric parameters, chemical abundances, and ages. Additional spectroscopic characterization of these stars (e.g. using the ESPRESSO ultra-high-resolution spectra) including derivation of different isotopic ratios will help to confirm or infirm their relation with the solar parent cluster.

*Acknowledgements.* This work was supported by Fundação para a Ciência e Tecnologia (FCT) through national funds (project ref. PTDC/FIS-AST/7073/2014, PTDC/FIS-AST/32113/2017, and PTDC/FIS-AST/32113/2017) and by Fundo Europeu de Desenvolvimento Regional (FEDER) through the COMPETE 2020 - Programa Operacional Competitividade e Internacionalização (POCI) (project ref. POCI-01-0145-FEDER-007672, POCI-01-0145-FEDER-032113). This work was also supported by FCT, POCI, FEDER in the framework of the project POCI-01-0145-FEDER-032113. V.A., E.D.M., N.C.S., and S.G.S. also acknowledge the support from FCT through Investigador FCT contracts nr. IF/00650/2015/CP1273/CT0001, IF/00849/2015/CP1273/CT0003, IF/00169/2012/CP0150/CT0002, and IF/00028/2014/CP1215/CT0002, respectively, and POPH/FSE (EC) by FEDER funding through the program “Programa Operacional de Factores de Competitividade - COMPETE”. V.A. also thanks the support from Observatoire de la Côte d’Azur (OCA) for the visitor program and would like to offer his special thanks to the OCA staff for all the support during his stay in Nice. P.deL., A.R.B. and G.K. acknowledge financial support from the ANR 14-CE33-014-01. ACSF is supported by grant 234989/2014-9 from CNPq (Brazil).

## References

- Adams, F. C. 2010, *ARA&A*, 48, 47
- Adams, F. C. & Spiegel, D. N. 2005, *Astrobiology*, 5, 497
- Adibekyan, V., Delgado-Mena, E., Feltzing, S., et al. 2017, *Astronomische Nachrichten*, 338, 442
- Adibekyan, V., Delgado-Mena, E., Figueira, P., et al. 2016, *A&A*, 591, A34
- Adibekyan, V., Figueira, P., Santos, N. C., et al. 2015a, *A&A*, 583, A94
- Adibekyan, V. Z., Benamati, L., Santos, N. C., et al. 2015b, *MNRAS*, 450, 1900
- Adibekyan, V. Z., González Hernández, J. I., Delgado Mena, E., et al. 2014, *A&A*, 564, L15
- Adibekyan, V. Z., Sousa, S. G., Santos, N. C., et al. 2012, *A&A*, 545, A32
- Alexeeva, S. A., Pakhomov, Y. V., & Mashonkina, L. I. 2014, *Astronomy Letters*, 40, 406
- Alvarez, R. & Plez, B. 1998, *A&A*, 330, 1109
- Andrássy, R. & Spruit, H. C. 2015, *A&A*, 579, A122
- Aoki, W., Frebel, A., Christlieb, N., et al. 2006, *ApJ*, 639, 897
- Arenou, F., Luri, X., Babusiaux, C., et al. 2018, *ArXiv e-prints* [[arXiv:1804.09375](https://arxiv.org/abs/1804.09375)]
- Armillotta, L., Krumholz, M. R., & Fujimoto, Y. 2018, *ArXiv e-prints* [[arXiv:1807.01712](https://arxiv.org/abs/1807.01712)]
- Asplund, M., Grevesse, N., Sauval, A. J., Allende Prieto, C., & Blomme, R. 2005, *A&A*, 431, 693
- Batista, S. F. A., Adibekyan, V. Z., Sousa, S. G., et al. 2014, *A&A*, 564, A43
- Batista, S. F. A. & Fernandes, J. 2012, *New A*, 17, 514
- Bedell, M., Meléndez, J., Bean, J. L., et al. 2014, *ApJ*, 795, 23

- Bensby, T., Feltzing, S., & Oey, M. S. 2014, *A&A*, 562, A71
- Bertran de Lis, S., Delgado Mena, E., Adibekyan, V. Z., Santos, N. C., & Sousa, S. G. 2015, *A&A*, 576, A89
- Bland-Hawthorn, J., Krumholz, M. R., & Freeman, K. 2010, *ApJ*, 713, L66
- Bobylev, V. V. & Bajkova, A. T. 2014, *Astronomy Letters*, 40, 353
- Bobylev, V. V., Bajkova, A. T., Mylläri, A., & Valtonen, M. 2011, *Astronomy Letters*, 37, 550
- Bonanno, A. & Fröhlich, H.-E. 2015, *A&A*, 580, A130
- Bovy, J. 2015, *ApJS*, 216, 29
- Bovy, J. 2016, *ApJ*, 817, 49
- Bressan, A., Marigo, P., Girardi, L., et al. 2012, *MNRAS*, 427, 127
- Brown, A. G. A., Portegies Zwart, S. F., & Bean, J. 2010, *MNRAS*, 407, 458
- Brown, M. E., Trujillo, C., & Rabinowitz, D. 2004, *ApJ*, 617, 645
- Cayrel, R. 1988, in *IAU Symposium*, Vol. 132, *The Impact of Very High S/N Spectroscopy on Stellar Physics*, ed. G. Cayrel de Strobel & M. Spite, 345
- Chabrier, G. 2001, *ApJ*, 554, 1274
- Chambers, J. E. 2010, *ApJ*, 724, 92
- Charbonnel, C. & Talon, S. 2005, *Science*, 309, 2189
- Cohen, J. G. 1968, *Astrophys. Lett.*, 2, 163
- Cosentino, R., Lovis, C., Pepe, F., et al. 2012, in *Proc. SPIE*, Vol. 8446, *Ground-based and Airborne Instrumentation for Astronomy IV*, 84461V
- da Silva, L., Girardi, L., Pasquini, L., et al. 2006, *A&A*, 458, 609
- de Laverny, P., Recio-Blanco, A., Worley, C. C., et al. 2013, *The Messenger*, 153, 18
- de Laverny, P., Recio-Blanco, A., Worley, C. C., & Plez, B. 2012, *A&A*, 544, A126
- De Pascale, M., Worley, C. C., de Laverny, P., et al. 2014, *A&A*, 570, A68
- Delgado Mena, E., Bertrán de Lis, S., Adibekyan, V. Z., et al. 2015, *A&A*, 576, A69
- Delgado Mena, E., Israelian, G., González Hernández, J. I., et al. 2014, *A&A*, 562, A92
- Delgado Mena, E., Tsantaki, M., Adibekyan, V. Z., et al. 2017, *A&A*, 606, A94
- Delgado Mena, E., Tsantaki, M., Zh. Adibekyan, V., et al. 2018, in *IAU Symposium*, Vol. 330, *IAU Symposium*, ed. A. Recio-Blanco, P. de Laverny, A. G. A. Brown, & T. Prusti, 156–159
- Dotter, A., Conroy, C., Cargile, P., & Asplund, M. 2017, *ApJ*, 840, 99
- Feng, Y. & Krumholz, M. R. 2014, *Nature*, 513, 523
- Flower, P. J. 1996, *ApJ*, 469, 355
- Gaia Collaboration, Brown, A. G. A., Vallenari, A., et al. 2018, *ArXiv e-prints* [[arXiv:1804.09365](https://arxiv.org/abs/1804.09365)]
- García-López, R. J., Rebolo, R., Beckman, J. E., & McKeith, C. D. 1993, *A&A*, 273, 482
- Gustafsson, B. 2018, *ArXiv e-prints* [[arXiv:1809.02361](https://arxiv.org/abs/1809.02361)]
- Gustafsson, B., Edvardsson, B., Eriksson, K., et al. 2008, *A&A*, 486, 951
- Hogg, D. W., Casey, A. R., Ness, M., et al. 2016, *ApJ*, 833, 262
- Jacobson, H. R., Friel, E. D., & Pilachowski, C. A. 2007, *AJ*, 134, 1216
- Kobayashi, C., Karakas, A. I., & Umeda, H. 2011, *MNRAS*, 414, 3231
- Kordopatis, G., Recio-Blanco, A., de Laverny, P., et al. 2011, *A&A*, 535, A106
- Kunitomo, M., Guillot, T., Ida, S., & Takeuchi, T. 2018, *ArXiv e-prints* [[arXiv:1808.07396](https://arxiv.org/abs/1808.07396)]
- Kupka, F., Piskunov, N., Ryabchikova, T. A., Stempels, H. C., & Weiss, W. W. 1999, *A&AS*, 138, 119
- Kurucz, R. L. 1993, *SYNTHES spectrum synthesis programs and line data*
- Lada, C. J. & Lada, E. A. 2003, *ARA&A*, 41, 57
- Lamers, H. J. G. L. M. & Gieles, M. 2006, *A&A*, 455, L17
- Lindegren, L., Hernandez, J., Bombrun, A., et al. 2018, *ArXiv e-prints* [[arXiv:1804.09366](https://arxiv.org/abs/1804.09366)]
- Liu, C., Ruchti, G., Feltzing, S., et al. 2015, *A&A*, 575, A51
- Liu, F., Asplund, M., Yong, D., et al. 2016a, *MNRAS*, 463, 696
- Liu, F., Yong, D., Asplund, M., Ramírez, I., & Meléndez, J. 2016b, *MNRAS*, 457, 3934
- Looney, L. W., Tobin, J. J., & Fields, B. D. 2006, *ApJ*, 652, 1755
- Lorenzo-Oliveira, D., Freitas, F. C., Meléndez, J., et al. 2018, *ArXiv e-prints* [[arXiv:1806.08014](https://arxiv.org/abs/1806.08014)]
- Lorenzo-Oliveira, D., Porto de Mello, G. F., & Schiavon, R. P. 2016, *A&A*, 594, L3
- Luri, X., Brown, A. G. A., Sarro, L. M., et al. 2018, *A&A*, 616, A9
- Mamajek, E. E. & Hillenbrand, L. A. 2008, *ApJ*, 687, 1264
- Martínez-Barbosa, C. A., Brown, A. G. A., Boekholt, T., et al. 2016, *MNRAS*, 457, 1062
- Masseron, T., Plez, B., Van Eck, S., et al. 2014, *A&A*, 571, A47
- Meléndez, J., Asplund, M., Gustafsson, B., & Yong, D. 2009, *ApJ*, 704, L66
- Meléndez, J., Ramírez, I., Karakas, A. I., et al. 2014, *ApJ*, 791, 14
- Mikolaitis, S., de Laverny, P., Recio-Blanco, A., et al. 2017, *A&A*, 600, A22
- Morbidelli, A. & Levison, H. F. 2004, *AJ*, 128, 2564
- Mortier, A., Santos, N. C., Sousa, S. G., et al. 2013, *A&A*, 558, A106
- Mortier, A., Sousa, S. G., Adibekyan, V. Z., Brandão, I. M., & Santos, N. C. 2014, *A&A*, 572, A95
- Ness, M., Rix, H.-W., Hogg, D. W., et al. 2018, *ApJ*, 853, 198
- Nissen, P. E. 2015, *A&A*, 579, A52
- Noyes, R. W., Hartmann, L. W., Baliunas, S. L., Duncan, D. K., & Vaughan, A. H. 1984, *ApJ*, 279, 763
- Pace, G. 2013, *A&A*, 551, L8
- Pagel, B. E. J. 1964, *Royal Greenwich Observatory Bulletins*, 87, 227
- Piskunov, A. E., Kharchenko, N. V., Röser, S., Schilbach, E., & Scholz, R.-D. 2006, *A&A*, 445, 545
- Piskunov, N. E., Kupka, F., Ryabchikova, T. A., Weiss, W. W., & Jeffery, C. S. 1995, *A&AS*, 112, 525
- Portegies Zwart, S. F. 2009, *ApJ*, 696, L13
- Ramírez, I., Asplund, M., Baumann, P., Meléndez, J., & Bensby, T. 2010, *A&A*, 521, A33
- Ramírez, I., Bajkova, A. T., Bobylev, V. V., et al. 2014, *ApJ*, 787, 154
- Recio-Blanco, A., Bijaoui, A., & de Laverny, P. 2006, *MNRAS*, 370, 141
- Reid, M. J., Menten, K. M., Brunthaler, A., et al. 2014, *ApJ*, 783, 130
- Ryabchikova, T., Piskunov, N., Kurucz, R. L., et al. 2015, *Phys. Scr.*, 90, 054005
- Santos, N. C., Israelian, G., & Mayor, M. 2004, *A&A*, 415, 1153
- Santos, N. C., Mayor, M., Bonfils, X., et al. 2011, *A&A*, 526, A112
- Santos, N. C., Mayor, M., Bouchy, F., et al. 2007, *A&A*, 474, 647
- Schilbach, E., Kharchenko, N. V., Piskunov, A. E., Röser, S., & Scholz, R.-D. 2006, *A&A*, 456, 523
- Schönrich, R., Binney, J., & Dehnen, W. 2010, *MNRAS*, 403, 1829
- Scott, P. C., Asplund, M., Grevesse, N., & Sauval, A. J. 2006, *A&A*, 456, 675
- Sestito, P. & Randich, S. 2005, *A&A*, 442, 615
- Slumstrup, D., Grundahl, F., Brogaard, K., et al. 2017, *A&A*, 604, L8
- Smalley, B. 2014, *Stellar Parameters from Photometry*, ed. E. Niemczura, B. Smalley, & W. Pych (Cham: Springer International Publishing), 111–120
- Smiljanic, R., Romano, D., Bragaglia, A., et al. 2016, *A&A*, 589, A115
- Smith, V. V., Cunha, K., & Lazzaro, D. 2001, *AJ*, 121, 3207
- Snedden, C., Pilachowski, C. A., & Vandenberg, D. A. 1986, *ApJ*, 311, 826
- Snedden, C. A. 1973, PhD thesis, THE UNIVERSITY OF TEXAS AT AUSTIN.
- Sousa, S. G. 2014, [[arXiv:1407.5817](https://arxiv.org/abs/1407.5817)] [[arXiv:1407.5817](https://arxiv.org/abs/1407.5817)]
- Sousa, S. G., Santos, N. C., Adibekyan, V., Delgado-Mena, E., & Israelian, G. 2015a, *A&A*, 577, A67
- Sousa, S. G., Santos, N. C., Mayor, M., et al. 2008, *A&A*, 487, 373
- Sousa, S. G., Santos, N. C., Mortier, A., et al. 2015b, *A&A*, 576, A94
- Sozzetti, A., Torres, G., Charbonneau, D., et al. 2007, *ApJ*, 664, 1190
- Spina, L., Meléndez, J., & Ramírez, I. 2016, *A&A*, 585, A152
- Suárez-Andrés, L., Israelian, G., González Hernández, J. I., et al. 2017, *A&A*, 599, A96
- Suárez Mascareño, A., Rebolo, R., & González Hernández, J. I. 2016, *A&A*, 595, A12
- Suárez Mascareño, A., Rebolo, R., González Hernández, J. I., & Esposito, M. 2015, *MNRAS*, 452, 2745
- Tepfer, D. & Leach, S. 2006, *Ap&SS*, 306, 69
- Théado, S. & Vauclair, S. 2012, *ApJ*, 744, 123
- Torres, G. 2010, *AJ*, 140, 1158
- Torres, G., Fischer, D. A., Sozzetti, A., et al. 2012, *ApJ*, 757, 161
- Tsantaki, M., Sousa, S. G., Adibekyan, V. Z., et al. 2013, *A&A*, 555, A150
- Tsantaki, M., Sousa, S. G., Santos, N. C., et al. 2014, *A&A*, 570, A80
- Tucci Maia, M., Ramírez, I., Meléndez, J., et al. 2016, *A&A*, 590, A32
- van Leeuwen, F. 2007, *A&A*, 474, 653
- von Bloh, W., Franck, S., Bounama, C., & Schellnhuber, H.-J. 2003, *Origins of Life and Evolution of the Biosphere*, 33, 219
- Weidner, C. & Kroupa, P. 2004, *MNRAS*, 348, 187
- Williams, J. P. & Gaidos, E. 2007, *ApJ*, 663, L33
- Wilson, T. L. & Matteucci, F. 1992, *A&A Rev.*, 4, 1
- Wolff, S. C., Heasley, J. N., & Varsik, J. 1985, *PASP*, 97, 707
- Worley, C. C., de Laverny, P., Recio-Blanco, A., Hill, V., & Bijaoui, A. 2016, *A&A*, 591, A81
- Worley, C. C., de Laverny, P., Recio-Blanco, A., et al. 2012, *A&A*, 542, A48
- Wright, J. T., Marcy, G. W., Butler, R. P., & Vogt, S. S. 2004, *ApJS*, 152, 261
- Yong, D., Lambert, D. L., Allende Prieto, C., & Paulson, D. B. 2004, *ApJ*, 603, 697

**Appendix A: Tables**

**Appendix B: Comparision of stellar parameters**

**Appendix C: Abundances**

**Table A.1.** Stellar parameters of the full sample stars and the S/N of the spectra used.

Star	$T_{\text{eff}}$	$\log g_{\text{spec}}$	$\log g_{\text{gaia}}$	[Fe/H]	$V_{\text{tur}}$	S/N
HD631	6048±28	4.40±0.04	4.39±0.01	0.08±0.02	1.07±0.04	70
HD2247	6269±29	4.42±0.04	4.42±0.01	0.04±0.02	1.32±0.04	113
HD4021	5764±25	4.49±0.04	4.50±0.01	0.06±0.02	1.11±0.03	178
HD6204	5843±16	4.49±0.03	4.52±0.01	0.04±0.01	1.05±0.02	708
HD6245	5167±25	3.03±0.07	3.03±0.01	0.03±0.02	1.29±0.03	433
HD6790	6030±19	4.46±0.03	4.41±0.01	0.05±0.01	1.04±0.03	251
HD7515	5889±21	4.52±0.03	4.51±0.01	-0.04±0.02	1.05±0.03	206
HD10180	5913±14	4.38±0.02	4.35±0.01	0.10±0.01	1.09±0.02	1639
HD10678	5609±20	4.38±0.04	4.50±0.01	0.10±0.02	0.88±0.03	69
HD22249	5737±20	4.54±0.04	4.55±0.01	-0.04±0.02	0.90±0.03	175
HD30858	5109±45	4.33±0.09	4.50±0.02	-0.07±0.03	0.66±0.10	84
HD37811	5146±31	2.91±0.08	2.78±0.01	0.01±0.03	1.55±0.03	307
HD38382	6076±13	4.45±0.03	4.37±0.01	0.04±0.01	1.19±0.02	1302
HD41071	5593±40	4.64±0.05	4.58±0.01	0.01±0.03	1.29±0.06	116
HD41842	5012±51	4.36±0.12	4.57±0.02	-0.02±0.03	0.81±0.12	201
HD45415	4830±47	2.67±0.10	2.60±0.04	-0.04±0.04	1.47±0.05	215
HD52456	5110±46	4.33±0.09	4.51±0.02	-0.02±0.03	0.65±0.11	108
HD56351	5734±19	4.63±0.02	4.56±0.01	-0.07±0.02	1.17±0.00	114
HD62412	4958±42	2.71±0.08	2.77±0.02	0.04±0.04	1.45±0.04	323
HD62816	6553±57	4.75±0.08	4.39±0.02	0.09±0.04	1.67±0.08	276
HD64942	5875±22	4.56±0.04	4.52±0.01	0.04±0.02	1.18±0.03	196
HD74006	5304±64	2.76±0.10	2.50±0.03	0.07±0.06	2.57±0.11	755
HD77191	5785±40	4.50±0.07	4.51±0.02	-0.02±0.03	1.19±0.06	180
HD89124	5668±18	4.45±0.03	4.51±0.01	-0.04±0.02	0.85±0.03	69
HD89839	6290±20	4.44±0.03	4.32±0.01	0.05±0.02	1.35±0.03	576
HD89965	4939±68	4.32±0.15	4.56±0.03	-0.08±0.04	0.53±0.21	318
HD92987	5860±15	4.18±0.02	4.12±0.01	0.07±0.01	1.16±0.02	424
HD95542	5971±17	4.48±0.03	4.48±0.01	-0.02±0.01	1.06±0.03	518
HD96116	5841±14	4.49±0.02	4.52±0.01	0.02±0.01	0.97±0.02	609
HD99648	5066±50	2.60±0.15	2.36±0.02	0.06±0.05	1.82±0.06	832
HD109098	5897±16	4.10±0.02	4.04±0.01	0.10±0.01	1.23±0.02	193
HD115341	6008±17	4.44±0.02	4.41±0.01	0.00±0.01	1.07±0.02	166
HD118563	5481±19	4.44±0.04	4.51±0.01	-0.03±0.01	0.79±0.03	204
HD126829	4535±108	4.28±0.30	4.58±0.04	-0.04±0.04	0.58±0.40	184
HD131218	5743±17	4.44±0.03	4.50±0.01	-0.02±0.01	0.91±0.03	107
HD136894	5406±16	4.34±0.03	4.45±0.01	-0.09±0.01	0.75±0.03	1204
HD155717	4942±55	4.46±0.13	4.60±0.02	-0.08±0.03	0.77±0.12	119
HD158469	6190±19	4.36±0.03	4.27±0.01	0.06±0.01	1.32±0.02	429
HD167554	5291±28	4.49±0.05	4.62±0.01	-0.07±0.02	0.90±0.06	270
HD176535	4635±46	4.38±0.18	4.57±0.02	-0.05±0.14	0.02±3.52	245
HD181387	6367±44	4.22±0.05	4.28±0.01	0.02±0.03	1.16±0.09	189
HD181517	4999±41	2.87±0.11	2.87±0.03	0.07±0.03	1.43±0.04	330
HD186302	5675±15	4.43±0.02	4.47±0.01	0.00±0.01	0.86±0.03	159
HD190204	5406±23	4.46±0.04	4.57±0.01	0.00±0.02	1.03±0.04	181
HD197300	5939±24	4.52±0.03	4.52±0.01	0.01±0.02	1.16±0.03	107
HD199951	5272±37	3.11±0.07	2.91±0.02	0.03±0.03	1.59±0.03	722
HD203387	5288±28	3.12±0.08	2.87±0.01	0.09±0.03	1.52±0.03	880
HD209458	6139±21	4.47±0.03	4.39±0.01	0.06±0.02	1.21±0.03	1114
HD212563	4946±53	4.37±0.15	4.57±0.02	0.00±0.03	0.71±0.13	124
HD216530	4750±84	4.27±0.22	4.55±0.03	0.02±0.04	0.74±0.22	85
HD218614	5666±20	4.48±0.03	4.52±0.01	-0.03±0.02	1.02±0.03	114
HIP96240	4767±55	4.25±0.15	4.56±0.02	-0.10±0.02	0.63±0.14	119
BD+004175B	6354±50	4.45±0.05	4.41±0.02	0.08±0.04	1.46±0.07	77
CoRoT-7	5309±37	4.42±0.09	4.56±0.02	0.02±0.03	0.96±0.07	566



**Table A.2.** Stellar mass, radius, age, and activity index for the full sample.

Star	$M_{star}$	$R_{star}$	$Age_{padova}$	$\log(R'_{HK})$
HD631	1.14±0.02	1.11±0.02	1.87±0.87	−4.93±0.06
HD2247	1.21±0.02	1.16±0.03	0.65±0.50	−5.29±0.13
HD4021	1.04±0.02	0.95±0.01	1.02±0.80	−4.36±0.03
HD6204	1.05±0.01	0.95±0.01	0.29±0.17	−4.49±0.03
HD6245	2.34±0.02	7.53±0.19	0.77±0.02	−4.84±0.05
HD6790	1.12±0.01	1.09±0.02	1.81±0.61	−4.80±0.01
HD7515	1.04±0.01	0.95±0.02	0.54±0.42	−4.42±0.02
HD10180	1.08±0.01	1.15±0.00	4.44±0.34	−4.92±0.01
HD10678	1.00±0.02	0.91±0.01	2.19±1.24	−4.67±0.01
HD22249	1.00±0.01	0.87±0.01	0.54±0.40	−4.49±0.02
HD30858	0.82±0.02	0.79±0.01	8.40±3.07	−4.60±0.08
HD37811	2.83±0.03	10.93±0.24	0.46±0.01	−5.28±0.01
HD38382	1.13±0.01	1.15±0.00	2.68±0.29	−4.89±0.02
HD41071	0.95±0.02	0.84±0.02	0.87±0.81	−4.31±0.02
HD41842	0.81±0.02	0.75±0.01	4.67±3.67	−4.37±0.09
HD45415	1.65±0.15	10.45±0.36	2.22±0.55	−5.43±0.01
HD52456	0.83±0.02	0.80±0.01	7.45±3.62	−4.72±0.01
HD56351	0.98±0.01	0.87±0.00	0.57±0.47	−4.35±0.04
HD62412	2.34±0.09	10.4±0.20	0.87±0.13	−5.20±0.03
HD62816	1.30±0.02	1.25±0.02	0.35±0.22	−4.77±0.03
HD64942	1.06±0.01	0.96±0.00	0.36±0.24	−4.42±0.04
HD74006	3.45±0.12	16.58±1.23	0.27±0.02	−5.06±0.02
HD77191	1.01±0.02	0.93±0.02	1.46±1.26	−4.37±0.01
HD89124	0.97±0.02	0.91±0.01	2.60±1.28	−4.62±0.04
HD89839	1.22±0.01	1.26±0.00	1.95±0.27	−4.98±0.10
HD89965	0.79±0.02	0.73±0.01	5.09±4.06	−4.66±0.04
HD92987	1.10±0.01	1.51±0.01	6.95±0.16	−4.89±0.00
HD95542	1.08±0.01	1.00±0.01	0.67±0.48	−4.64±0.06
HD96116	1.05±0.01	0.95±0.01	0.33±0.21	−4.61±0.04
HD99648	3.66±0.11	19.92±1.38	0.23±0.02	−4.77±0.00
HD109098	1.18±0.01	1.69±0.04	5.52±0.23	−4.98±0.05
HD115341	1.09±0.01	1.07±0.03	2.67±0.52	−4.90±0.15
HD118563	0.91±0.02	0.87±0.01	4.79±1.76	−4.69±0.02
HD126829	0.71±0.01	0.66±0.01	4.83±3.98	−4.44±0.02
HD131218	1.00±0.02	0.91±0.01	1.85±1.06	−4.68±0.15
HD136894	0.85±0.01	0.87±0.01	11.08±0.55	−4.93±0.01
HD155717	0.77±0.02	0.72±0.01	4.50±3.93	−4.52±0.03
HD158469	1.20±0.00	1.32±0.01	3.03±0.18	−4.95±0.02
HD167554	0.86±0.01	0.76±0.00	0.71±0.68	−4.34±0.02
HD176535	0.75±0.02	0.69±0.02	5.64±4.10	−4.81±0.04
HD181387	1.25±0.02	1.34±0.03	2.00±0.41	−5.06±0.04
HD181517	2.33±0.13	9.33±0.31	0.84±0.16	−5.38±0.06
HD186302	0.97±0.01	0.95±0.01	4.50±0.81	−4.84±0.06
HD190204	0.92±0.02	0.83±0.02	1.31±1.16	−4.37±0.03
HD197300	1.07±0.01	0.96±0.00	0.37±0.25	−4.36±0.02
HD199951	2.57±0.05	9.03±0.32	0.60±0.03	−4.65±0.03
HD203387	2.67±0.03	9.64±0.29	0.55±0.02	−4.72±0.01
HD209458	1.17±0.02	1.14±0.02	1.42±0.56	−4.91±0.01
HD212563	0.80±0.02	0.75±0.02	4.83±3.83	−4.31±0.01
HD216530	0.77±0.02	0.72±0.01	5.00±3.95	−4.33±0.00
HD218614	0.98±0.02	0.89±0.02	1.81±1.19	−4.37±0.00
HIP96240	0.75±0.02	0.70±0.01	5.97±4.19	−4.54±0.03
BD+004175B	1.22±0.02	1.16±0.02	0.56±0.42	−5.02±0.09
CoRoT-7	0.89±0.02	0.81±0.02	2.93±2.64	−4.82±0.07
NAME TrES-1	0.88±0.01	0.91±0.01	10.15±1.37	−4.79±0.00

**Table A.3.** Kinematic parameters of the full sample stars.

Star	RV	$U_{LSR}$	$V_{LSR}$	$W_{LSR}$	Z	R	$e$	$Z_{max}$	$R_{per}$	$R_{ap}$
HD631	31.9	-5.5	23.1	-22.0	-0.026	8.354	0.122	0.401	10.662	8.342
HD2247	20.6	6.4	4.8	-14.7	-0.115	8.336	0.034	0.261	8.860	8.275
HD4021	-3.0	11.2	15.5	10.8	-0.034	8.344	0.088	0.178	9.872	8.275
HD6204	-3.0	8.7	14.6	11.4	-0.026	8.351	0.081	0.184	9.769	8.306
HD6245	-1.5	9.9	16.5	7.2	-0.046	8.329	0.090	0.125	9.923	8.277
HD6790	-23.8	-1.5	20.2	29.3	-0.071	8.335	0.109	0.566	10.375	8.334
HD7515	1.0	24.2	5.4	10.9	-0.050	8.327	0.087	0.177	9.374	7.871
HD10180	35.4	20.4	-3.7	-23.3	-0.007	8.332	0.071	0.379	8.832	7.666
HD10678	16.0	15.9	-3.5	-1.4	-0.013	8.332	0.056	0.025	8.673	7.746
HD22249	15.9	4.9	-3.7	0.3	-0.017	8.348	0.025	0.017	8.402	7.990
HD30858	25.9	-0.6	1.2	-13.8	-0.006	8.368	0.008	0.204	8.506	8.366
HD37811	-5.6	31.5	13.8	-1.9	-0.030	8.395	0.129	0.048	10.301	7.951
HD38382	37.8	-16.8	-8.3	-8.0	0.015	8.357	0.070	0.117	8.612	7.488
HD41071	24.9	-0.1	-9.8	1.0	0.000	8.355	0.049	0.014	8.355	7.572
HD41842	12.4	0.0	6.8	2.2	0.012	8.360	0.035	0.034	8.961	8.360
HD45415	52.7	-39.7	0.4	-10.4	0.019	8.421	0.135	0.169	9.749	7.434
HD52456	-12.0	19.5	22.3	4.1	0.028	8.365	0.131	0.077	10.710	8.225
HD56351	-5.0	18.8	16.2	9.3	0.008	8.344	0.105	0.151	10.090	8.173
HD62412	-16.1	31.7	20.8	-0.9	0.023	8.388	0.152	0.031	10.918	8.043
HD62816	-4.5	16.5	14.7	8.5	0.032	8.378	0.094	0.142	9.942	8.230
HD64942	-8.4	23.4	13.7	7.2	0.033	8.372	0.106	0.122	10.017	8.091
HD74006	-11.4	28.7	19.9	4.0	0.032	8.366	0.141	0.078	10.707	8.064
HD77191	-7.5	14.2	17.0	0.8	0.059	8.380	0.099	0.069	10.106	8.280
HD89124	-4.0	17.4	18.3	7.7	0.012	8.319	0.110	0.126	10.206	8.184
HD89839	31.9	15.3	-19.7	11.3	0.028	8.329	0.111	0.167	8.442	6.759
HD89965	-7.0	8.1	20.6	8.5	0.042	8.342	0.108	0.149	10.331	8.314
HD92987	4.5	13.0	9.7	14.1	0.038	8.335	0.067	0.227	9.384	8.203
HD95542	15.4	15.3	-3.7	9.6	0.019	8.320	0.055	0.142	8.640	7.745
HD96116	31.3	31.1	-14.9	0.5	0.027	8.321	0.128	0.029	8.816	6.812
HD99648	-8.8	28.8	14.5	0.1	0.159	8.354	0.124	0.186	10.231	7.981
HD109098	2.0	1.3	15.4	13.5	0.075	8.329	0.079	0.236	9.766	8.328
HD115341	19.4	21.5	-4.7	18.0	0.065	8.322	0.076	0.292	8.806	7.569
HD118563	-18.9	-8.7	17.3	1.1	0.047	8.305	0.092	0.056	9.941	8.266
HD126829	-18.4	-3.6	15.8	-3.4	0.048	8.316	0.081	0.075	9.769	8.309
HD131218	24.9	23.4	-11.0	3.8	0.008	8.306	0.096	0.055	8.671	7.151
HD136894	-6.4	6.3	10.2	0.6	0.036	8.317	0.055	0.040	9.255	8.283
HD155717	12.5	20.5	14.8	15.8	0.043	8.297	0.103	0.267	9.951	8.087
HD158469	39.3	50.8	5.2	18.3	0.021	8.274	0.174	0.319	10.268	7.220
HD167554	21.9	32.4	13.7	-0.2	0.014	8.283	0.130	0.017	10.154	7.821
HD176535	-31.9	-15.9	-5.5	13.6	0.020	8.306	0.060	0.203	8.596	7.623
HD181387	-32.0	-2.8	-25.4	8.2	0.009	8.221	0.129	0.116	8.225	6.348
HD181517	10.0	15.6	8.9	-6.7	-0.040	8.215	0.069	0.110	9.204	8.020
HD186302	-1.0	8.4	2.5	13.8	-0.004	8.300	0.032	0.206	8.688	8.154
HD190204	13.0	25.0	22.0	4.4	-0.009	8.285	0.139	0.073	10.677	8.064
HD197300	-13.9	-7.9	7.3	4.2	-0.009	8.294	0.045	0.062	9.002	8.223
HD199951	19.0	27.8	10.9	-2.9	-0.019	8.289	0.109	0.051	9.801	7.872
HD203387	12.4	11.2	18.9	-6.6	-0.015	8.301	0.103	0.107	10.133	8.244
HD209458	-15.0	4.0	-3.6	7.7	0.002	8.330	0.022	0.110	8.370	8.002
HD212563	-13.4	2.3	1.0	14.9	-0.012	8.319	0.010	0.221	8.461	8.289
HD216530	14.0	16.0	16.9	-6.4	-0.016	8.318	0.101	0.104	10.044	8.193
HD218614	7.9	19.8	22.0	5.2	-0.022	8.327	0.130	0.090	10.633	8.182
HIP96240	5.0	12.4	22.2	4.7	0.009	8.295	0.119	0.077	10.465	8.235
BD+004175B	-47.0	-14.6	-34.5	9.8	0.009	8.221	0.180	0.140	8.283	5.759
CoRoT-7	31.2	-11.0	-8.0	13.5	0.019	8.474	0.053	0.204	8.611	7.748
NAME TrES-1	-20.7	20.7	-18.6	18.0	0.062	8.282	0.115	0.284	8.491	6.744

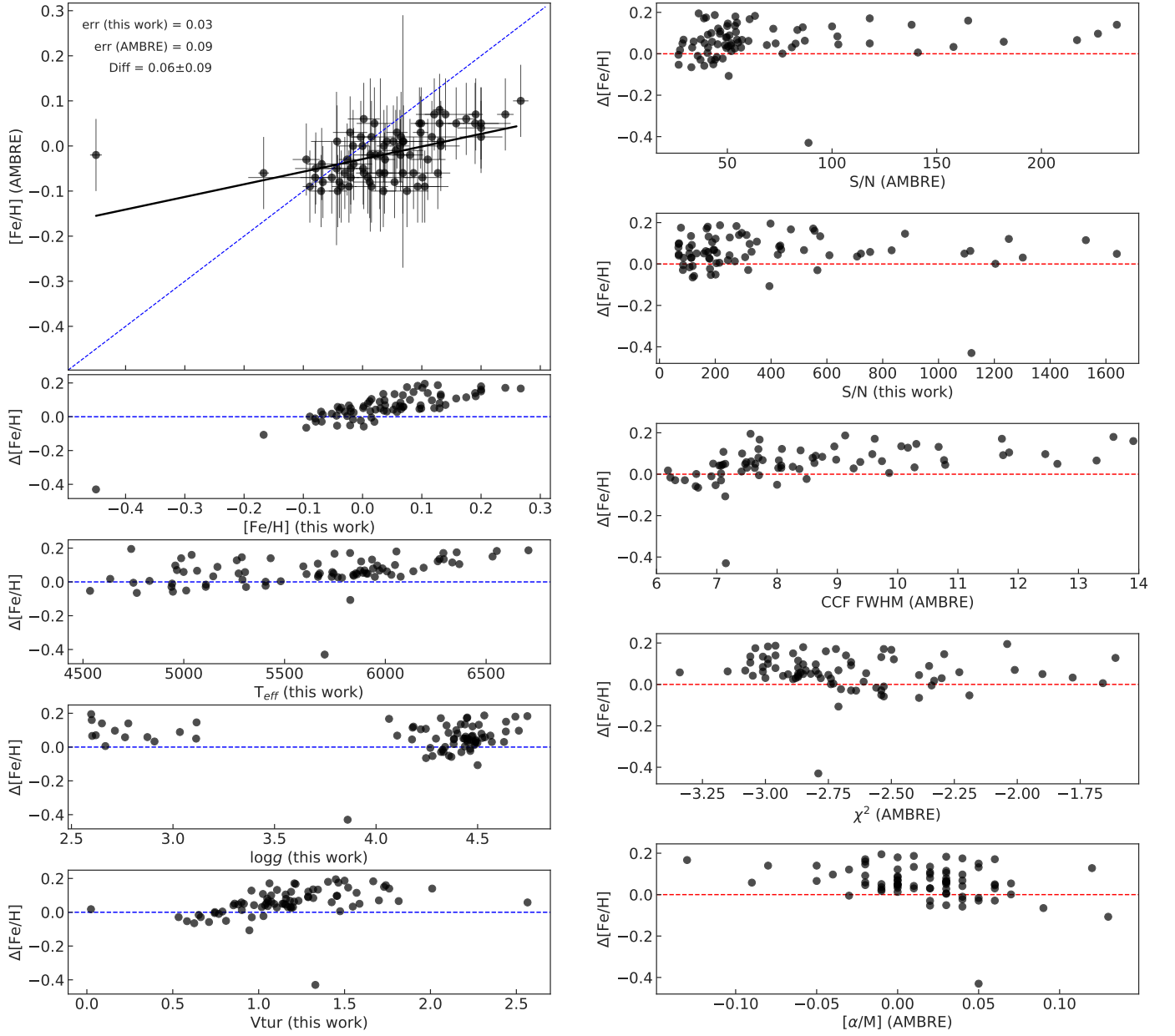


**Fig. B.1.** Comparison of the stellar mean metallicities derived within the AMBRE project and  $[\text{Fe}/\text{H}]$  derived in the present work.

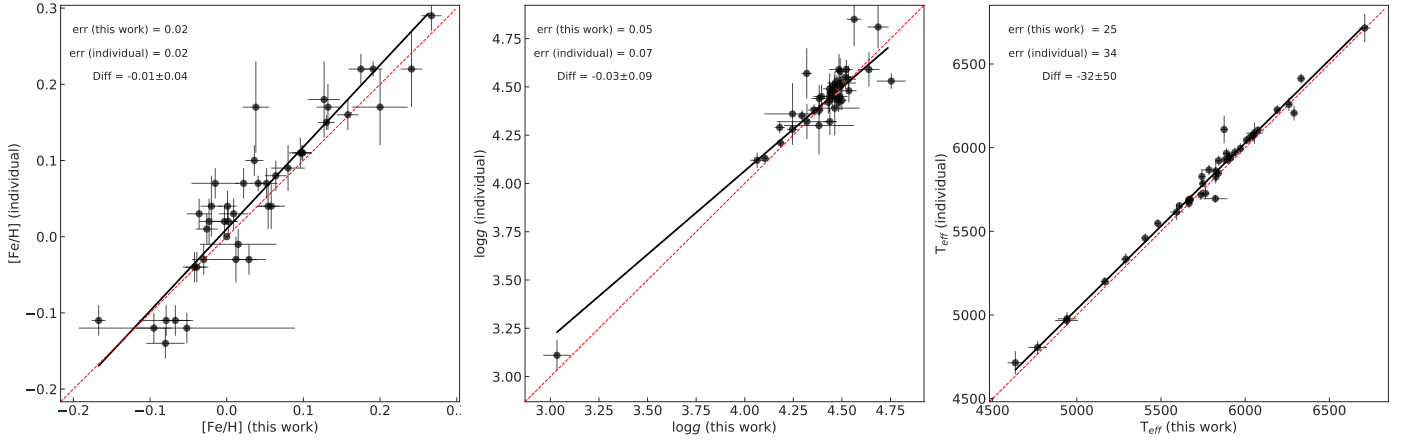


**Fig. B.2.** Comparison of the stellar parameters derived within the AMBRE project and in the current work. In both works, the parameters are derived from the same individual single spectrum.

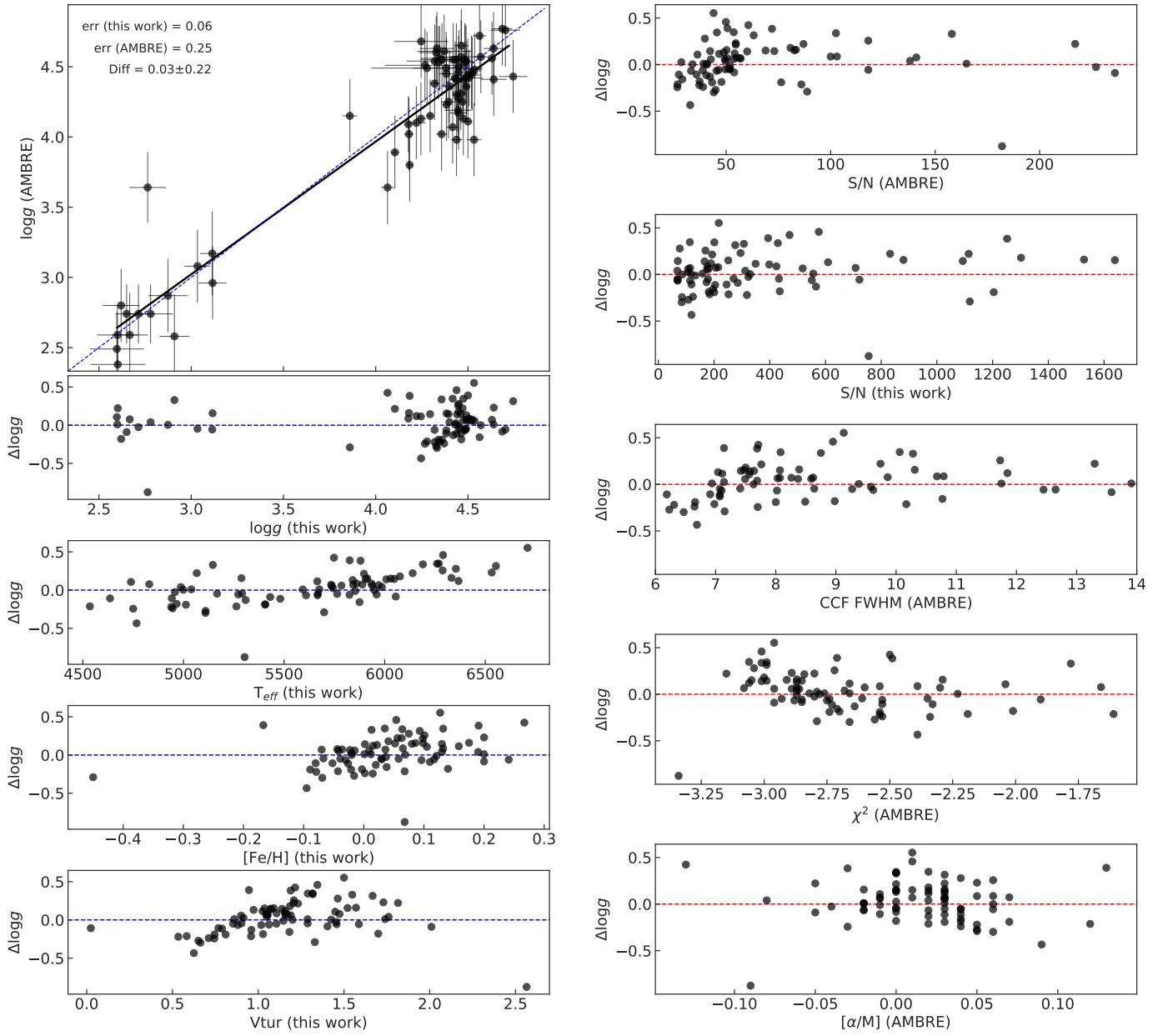


**Fig. B.3.** Comparison of the surface gravities derived within the AMBRE project and derived in the present work.



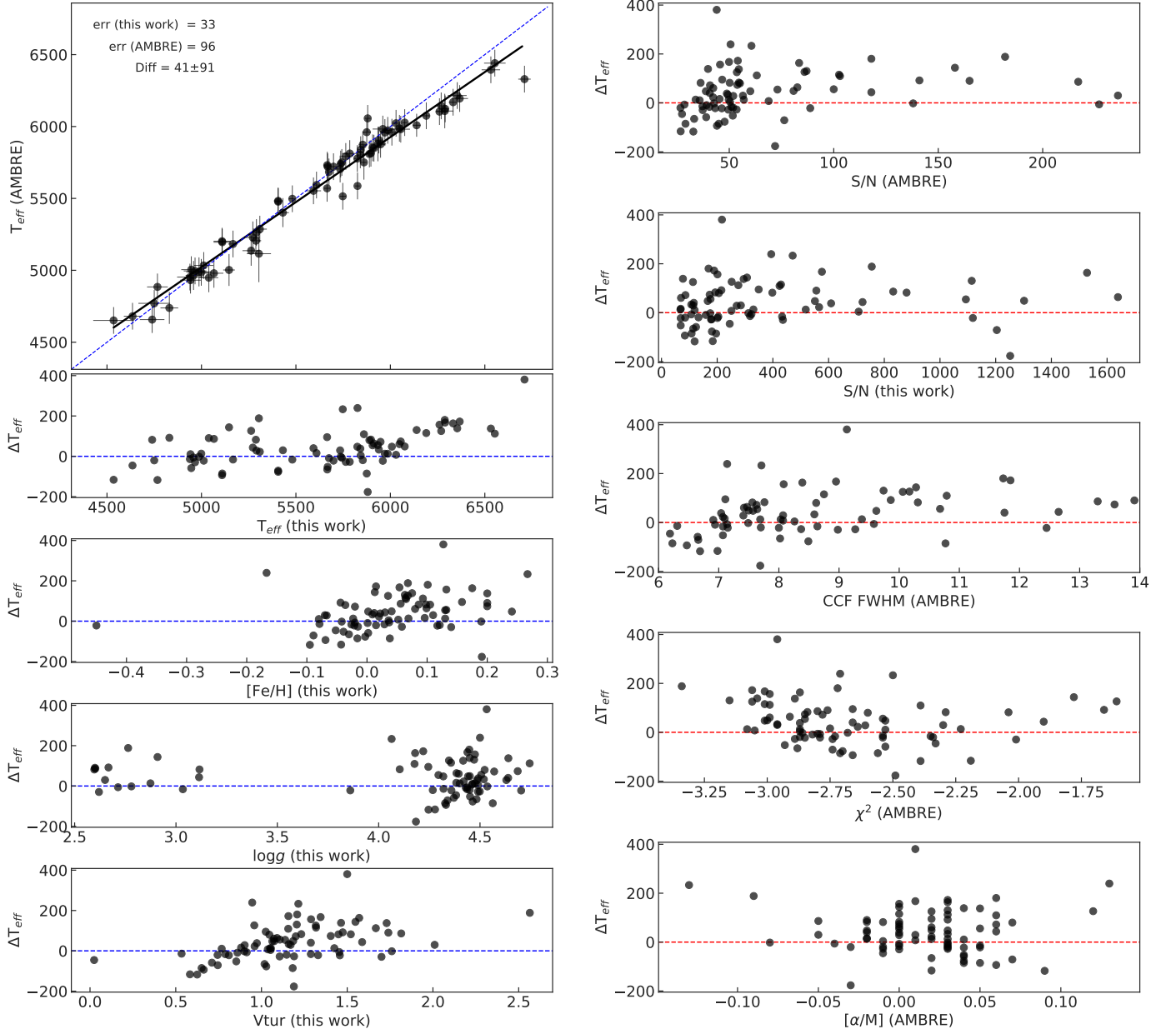


**Fig. B.4.** Comparison of the stellar effective temperatures derived within the AMBRE project and derived in the present work.

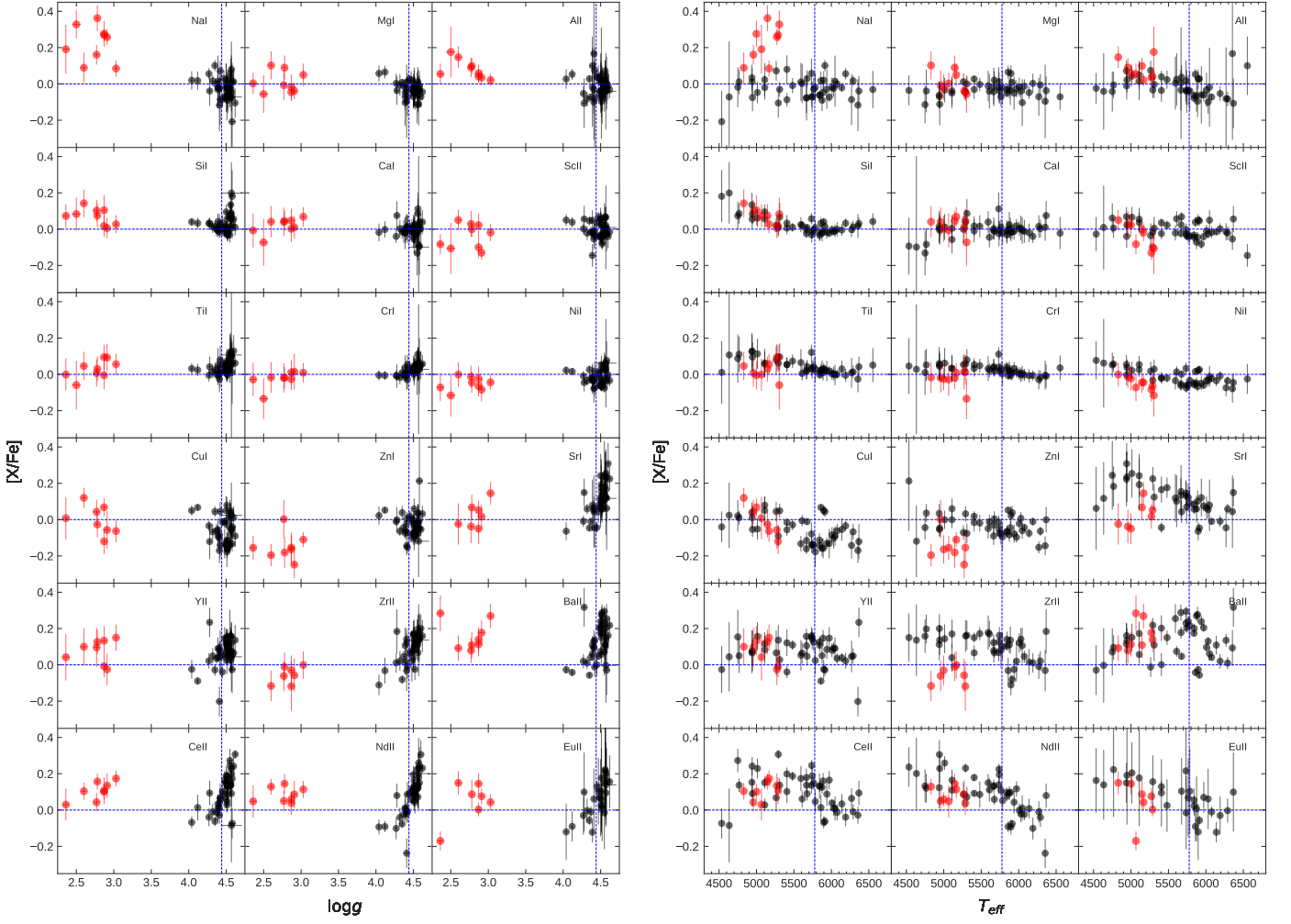


**Fig. C.1.** Abundance ratio  $[X/Fe]$  against trigonometric  $\log g$  and  $T_{\text{eff}}$  for the current sample. The evolved (also massive) stars with surface gravity smaller than 3.5 dex are represented in red colour, and the stars at earlier stages of their evolution are shown in black. The blue dashed horizontal and vertical lines show the solar abundances.

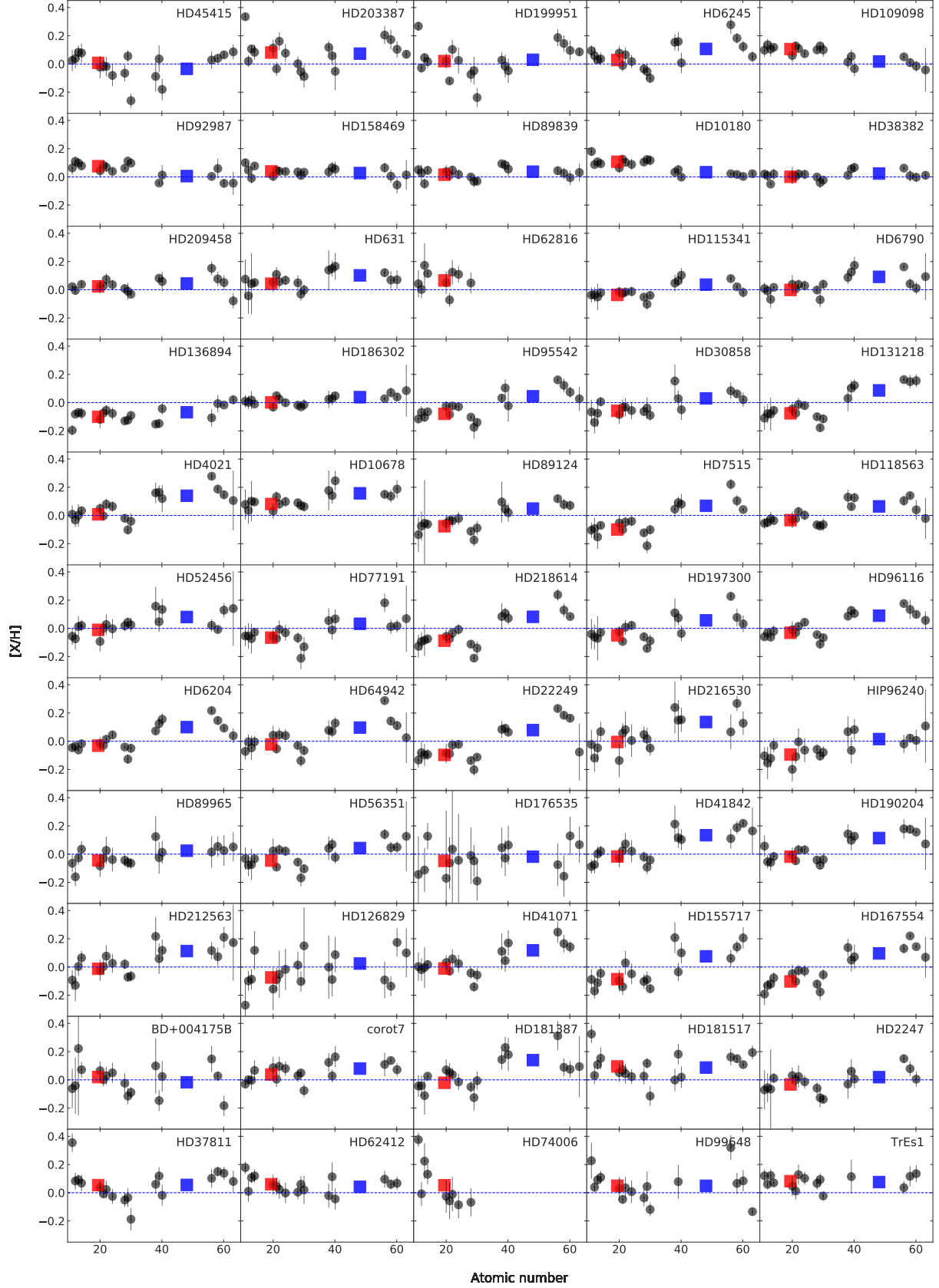


**Fig. C.2.** Abundances versus atomic number for the sample stars. The average abundances of light ( $Z \leq 30$ ) and heavy ( $Z > 30$ ) elements are shown by red and blue squares, respectively.